

On the Phenomenology of Hidden Valleys with Heavy Flavor

Matthew J. Strassler

Department of Physics and Astronomy, Rutgers University, Piscataway, NJ 08854

A preliminary investigation of a large class of Hidden Valley models is presented. These models are more challenging than those considered in arXiv:0712.2041 [hep-ph]; although they produce a new light resonance which decays to heavy standard model fermions, they exhibit no light dilepton resonance. A heavy Z' decaying to v -hadrons, which in turn decay mainly to bottom quarks and tau leptons, is considered; six case studies are investigated, using a new Monte Carlo simulation package. It is found that the one-to-one correspondence of jets and partons is badly broken, and the high-multiplicity heavy-flavor signal probably cannot be isolated by counting jets, with or without heavy-flavor tags. Instead, other measures, such as counting and correlating vertices or displaced tracks, and possibly counting of (non-isolated) muons and use of event-shape variables, should be combined with scalar transverse energy and/or missing transverse energy to reduce backgrounds. Within the resulting sample, searches for the v -pion mass resonance in both di-jet and single-jet invariant mass can help confirm a signal. The best observable in a perfect calorimeter seems to be single-jet invariant mass for jets of larger radius ($R=0.7$), although this needs further study in a realistic setting. A more detailed signal-to-background study is needed as a next step, but will face the difficulty of estimating the various high-multiplicity backgrounds.

I. INTRODUCTION

The “Hidden Valley” scenario [1], if realized in nature, may result in unusual and little-studied phenomena at the LHC. In this scenario, the standard model is accompanied by a nearly hidden sector containing light particles (a “hidden valley”). These particles cannot currently be abundantly produced, due typically to an energetic barrier or a weak coupling. The increased energy of the LHC may greatly enhance their production. The same barrier can be traversed in the opposite direction to allow some of these particles to decay visibly to standard model particles. A schematic illustration of such models is shown in Fig. 1. Examples of hidden valley models include the original illustrative classes of models given in [1], along with quirk and squirk models [1, 2, 3, 4] and a wide class of “unparticle” models [5] with an added mass gap (e.g. [6, 7]), whose signals were discussed in detail in [8]. Another related class of examples was studied in [9, 10, 11]. Motivation for such sectors is provided by, among other possibilities, supersymmetry-breaking models, which often introduce one or more hidden gauge groups. While these gauge groups are normally imagined to be unimportant at LHC energies, this reflects a theoretical bias. Such sectors might also be responsible for dark matter, and may have an important role to play in other aspects of particle physics [12], astrophysics and cosmology [13].

The main interest of these models for the LHC era is that their signatures are often distinctive, and can differ from the many supersymmetry, little Higgs, extra-dimensional and technicolor signatures that have been so often discussed. These include high-multiplicity events (generally non-thermal and non-spherical), possibly with large missing energy, and exhibiting large event-to-event fluctuations. New decay modes for Higgs bosons [1, 8, 14], supersymmetric particles [8, 15], and top quarks [8] often arise. Light neutral resonances are common, lighter

perhaps than 100 GeV or even 10 GeV.

A common hidden valley signature, but one which I will *not* address in this paper, is displaced vertices. In certain regions of parameter space, some of the new light particles have long lifetimes, decaying at macroscopic distances. There is no standard model background to compute or estimate. Key issues associated with such signals involve experimental challenges: triggering, detector noise, beam halo, pion collisions with detector material, vertex reconstruction, *etc.* All of these are detector-specific, and any study of this signature requires a full detector simulation.

However, it may happen that all the new particles decay promptly, or that some decay promptly and all others are stable and invisible. In this case, identifying the resulting high-multiplicity and often low-rate signal, over a large standard model background, becomes a challenge that can be addressed in part through theory and simulation. Below I will consider models of this type.

In some classes of hidden valley models [1, 8], there is a new and frequently-produced particle that often decays to electron and muon pairs. It is then relatively easy to discover the signal, as emphasized in [16]. Simple and rather crude event-shape cuts that remove the largest backgrounds may enhance signal-to-background to the point that, using the excellent low- p_T dilepton mass resolution of the LHC experiments, a resonant peak could be detected.

In this paper, I will consider a much more difficult situation. I will examine a class of hidden valley models *with prompt decays and heavy-flavor final states, and with no dilepton resonances*. Some of these models also have large missing energy. All have large event-to-event fluctuations in the multiplicity of standard model partons in the final state. The background to such signals is difficult to estimate, because it consists of a cocktail of many different processes, none of which can be calculated beyond leading order in α_s , and few of which can be identified and

measured using the data itself. Because of this, it will be a considerable challenge to carry out a concrete signal-to-background study. The goal of this article is to lay the groundwork for such a study, and suggest features of the signal which could be used in any search for a hidden valley of this type.

First I will outline the specific model that is chosen as an exemplar from this class, and will describe the Monte Carlo event generation package used to study it. Then I will describe the case studies, examining the basic phenomenological features of the signal, in Sec. II. After exploring the basic underlying phenomena, I will consider how jets are constructed in the signal. Finding that jets are not fully sufficient for interpreting or isolating the signal, I will consider other non-standard methods for reducing background. Finally, in Sec. III, I will examine the question of how to identify the resonance whose observation would confirm the signal, considering both dijet and single jet invariant mass. A summary of results and some additional comments are given in the conclusion; two appendices fill in some details on secondary muons and on jet algorithms.

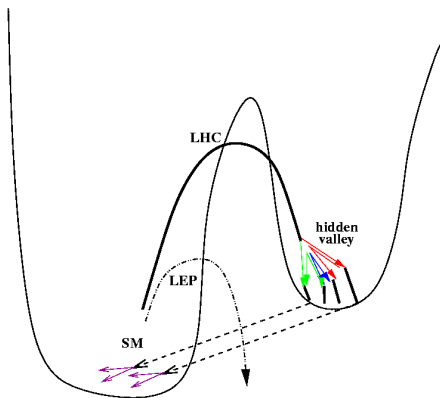


FIG. 1: A schematic illustration of models in the hidden-valley scenario. With sufficient energy, available at the LHC but not at LEP, a barrier may be traversed that allows production of new light states in a hidden sector. Dynamics in the hidden sector may produce large numbers of particles. Some of these new particles may decay back to the standard model, often with long lifetimes.

A. The Models

Several large classes of hidden valley models share the phenomenology of high-multiplicity final states, rich in heavy flavor and possibly missing energy. These include a wide variety of confining hidden sectors whose light stable hadrons are all pseudoscalar and/or scalar mesons with comparable masses; an example was given in [1]. Another class involves weakly-coupled models with multiple

electroweak doublet and singlet Higgs bosons which mix together. These models have been discussed widely (see [7] and references therein) but their potential for high-multiplicity heavy-flavor final states was only recently recognized [8, 14, 17]. A third class can include strongly-interacting hidden valleys which couple to the standard model mainly through the Higgs boson; these have not yet been explored fully.

In this paper I will consider the theory in [1], as a very simple example from the first category. This is a hidden valley which closely resembles QCD. To make this study especially straightforward, I have chosen a hidden valley sector (“v-sector”) that, like QCD, has an $SU(3)$ gauge group and two light “v-quarks” U and D , with masses adjusted so that the light “v-hadron” mass ratios are those of QCD. It is important to emphasize that this model is a stand-in for a much larger class of models. Indeed there is no reason for the physics of a hidden valley to closely resemble QCD, any more than technicolor models should closely resemble QCD. However, for initial studies of v-sector phenomenology, the case of a QCD-like v-sector is simplest to investigate first. This is because the physics is easy to understand, and a Monte Carlo event simulator is easily constructed.

As in [1], where more details are given, I will consider such a v-sector coupled to the standard model through a broken $U(1)$ gauge symmetry, under which both standard model particles and the v-quarks carry a charge. The Z' gauge boson of the $U(1)$ will serve to mediate both production and decay of particles in the v-sector.

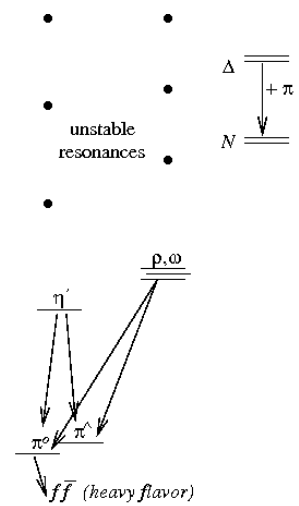


FIG. 2: The spectrum of the v-sector considered in this paper. In analogy to QCD, all v-hadrons rapidly decay down to v-pions and v-nucleons; then the π_v^0 (and in the B cases, also the π_v^Δ and π_v^∇) decay more slowly to standard model fermion pairs, preferentially to heavy flavor.

The long-lived v-hadrons of a QCD-like v-sector with two light v-quarks U and D are three light v-pions and a

heavier v -nucleon doublet, as shown in Fig. 2. All other v -hadrons (such as the v -rho and v -Delta) decay immediately to v -pions and v -nucleons. For simplicity, it is assumed that v -baryon number is conserved, so the v -nucleons are stable and invisible. The three v -pions π_v , a triplet under v -isospin, consist of a v -flavor off-diagonal pair with quantum numbers of $U\bar{D}$ and $D\bar{U}$, analogous to the π^\pm of QCD, and a third, the v -flavor diagonal v -pion with quantum numbers of $U\bar{U} - D\bar{D}$, analogous to the π^0 .

A point of notation: it is natural to name the v -pions as (π_v^\pm, π_v^0) , in analogy to QCD's pions (π^\pm, π^0) . This notation was used in [1]. However, the use of the \pm superscript proves confusing, because *all the v -pions are electrically neutral* — after all, they are part of a hidden sector. To avoid any confusion of this type (and at the expense of introducing another), I will call the $U\bar{U} - D\bar{D}$ state π_v^0 , but call the $U\bar{D}$ state π_v^\wedge , and the conjugate $D\bar{U}$ state π_v^\vee .



FIG. 3: The π_v^0 decays via a Z' to heavy flavor. The π_v^\wedge , if unstable, decays through a v -flavor-changing interaction to the same final state.

If the third component of v -isospin I_v^3 is conserved, then the π_v^\wedge is stable and invisible, but the breaking of total v -isospin allows the π_v^0 to decay via a Z' back to standard model particles, as shown in Fig. 3. Helicity suppression assures the spin-zero π_v^0 decays mainly to heavy fermions (for the same reason that $\pi^+ \rightarrow \mu^+\nu$ decays dominate over $\pi^+ \rightarrow e^+\nu$ in QCD); branching fractions are roughly proportional to squares of fermion masses. In the particular model of [1], and for light v -pion masses, the width of the π_v^0 is

$$\Gamma_{\pi_v^0} \sim 6 \times 10^9 \text{ sec}^{-1} \frac{f_{\pi_v}^2 m_{\pi_v}^5}{(20 \text{ GeV})^7} \left(\frac{10 \text{ TeV}}{m_{Z'}/g'} \right)^4. \quad (1)$$

which has a very strong dependence on model parameters; here f_{π_v} is the v -pion decay constant, while $m_{Z'}$ and g' are the Z' mass and coupling.

It is also possible that the third component of v -isospin I_v^3 is violated. In this case even the π_v^\wedge and π_v^\vee can decay, with widths that are smaller than that of the π_v^0 by a factor which is a dimensionless measure of I_v^3 breaking. In this article, I simply assume that *either* (A) I_v^3 is conserved (so that the π_v^\wedge is stable and invisible) *or* (B) I_v^3 is badly violated (so that the π_v^\wedge decays promptly.) The case studies will be divided into “A cases” and “B cases” according to this distinction.

The basic production process for these particles is shown in Fig. 4. It involves $q\bar{q} \rightarrow Z' \rightarrow Q\bar{Q}$, where Q is a

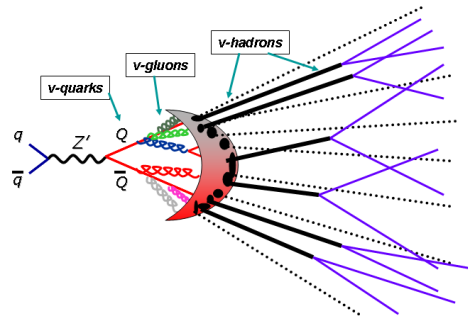


FIG. 4: A Z' decays to two v -quarks, which emit v -gluons in a v -parton shower. These then are confined into v -pions and v -nucleons. Some of the v -hadrons (shown dotted) are stable and invisible, but others are metastable and decay, mainly to $b\bar{b}$.

v -quark. The v -quarks undergo a parton shower through v -gluon emission, following which they are confined by strong v -interactions into v -hadrons. These v -hadrons decay down to v -nucleons and v -pions, and some of the v -pions may then decay visibly to standard model particles.

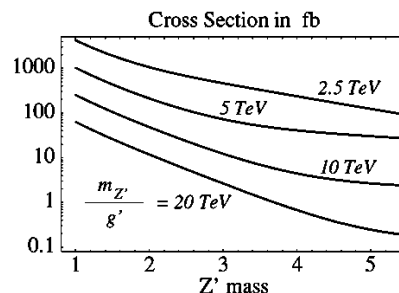


FIG. 5: Cross-section for v -particle production via a Z' in the QCD-like model of [1]. The cross-section in other models may easily differ by an order of magnitude; see text.

In the study below, I will consider a Z' with mass 3.2 TeV. The v -pion masses will range between 50 and 200 GeV. In this case the v -pions decay promptly, and the production cross-section is expected to be of order 10–100 fb in the model of [1], see Fig. 5. In other models the cross-section could be different by a factor of 10 or so, larger or smaller, due for example to different Z' charge assignments, or to a different number of colors in the v -sector.

In summary, the model considered below has gauge group $[SU(3) \times SU(2) \times U(1)]_{SM} \times U(1)' \times SU(3)_v$, with the $U(1)'$ broken at the few TeV scale, the $SU(3)_v$ group confining at the few hundred GeV scale, and two light v -flavors of v -quarks U and D . Standard model fermions

and v-quarks all carry some charge under the $U(1)'$, allowing the Z' to serve as a communicator between the two sectors.

B. The Hidden Valley Monte Carlo 0.5

The event simulator HVMC 0.5, upon which all studies in this paper are based, is described in this section. (A more general Monte Carlo simulator has been developed with S. Mrenna and P. Skands [18], and studies based upon it will be presented elsewhere.) HVMC 0.5 [19] is built on existing tools, which are rather easy to modify for current purposes. In particular, elements of PYTHIA [20] are strung together to simulate a v-sector which is isomorphic to three-color two-flavor QCD, with all masses and other dimensional quantities scaled up, relative to QCD, by a constant factor R .

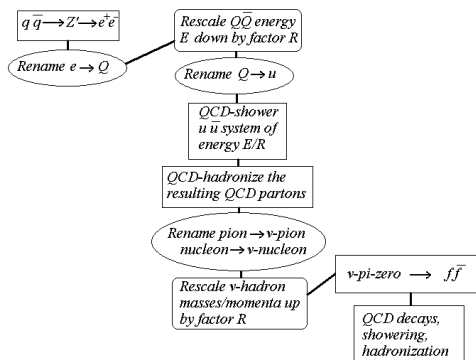


FIG. 6: The algorithm used in HVMC 0.5.

A v-sector with three colors, two flavors and confinement scale Λ_v has v-pions with mass $m_{\pi_v} = m_{\pi}R$, where $R \equiv \Lambda_v/\Lambda_{QCD}$, and Λ_{QCD} is the QCD confinement scale. It also has nucleons with similarly scaled-up masses. The η'_v (the iso-singlet pseudoscalar of 2-flavor QCD) has its mass set to $m_{\eta}R$. Then, given a mass M for the Z' , the simulation of events proceeds as in Fig. 6.

- The process $q\bar{q} \rightarrow Z' \rightarrow Q\bar{Q}$ is simulated, where q is an ordinary quark and Q is a v-quark, using the PYTHIA routine for $q\bar{q} \rightarrow Z' \rightarrow f\bar{f}$.
- The v-parton showering and v-hadronization of the $Q\bar{Q}$ system is simulated. This is done by
 - scaling down the energy of the $Q\bar{Q}$ system from its original energy E_0 to the energy $E = E_0/R$;
 - simulating QCD parton showering and hadronization (with the number of light flavors set to 2) of an ordinary quark-antiquark system with center-of-mass energy equal to E ;

- scaling up the masses and momenta of the final-state QCD hadrons (with π^0 's undecayed) by the factor R , and renaming them as v-hadrons.

- The decay of the v-hadrons to standard model partons is simulated using PYTHIA decay routines.
- The decays, showering and hadronization of the standard model partons and the simulation of the underlying event proceed using the usual PYTHIA routines.

The resulting final states consist of standard model hadrons, photons and leptons, along with stable neutral v-hadrons that escape undetected. *All results in this paper are based on analysis of the final state hadrons, photons and leptons without accounting for detector effects, other than geometric acceptance, except where otherwise noted.*

For the sake of clarity (though the actual effect on the studies below is small) it should be noted that two-flavor QCD as simulated in this way is not quite a consistent model. The tuning of PYTHIA to match existing data on hadronization, branching fractions, *etc.*, is not correct for a two-flavor model. The iso-singlet would-be Nambu-Goldstone boson η_v is now affected by the anomaly and takes the place of the η' . There are small effects on the nucleon mass from the slight differences in the running coupling that are similarly ignored. But these issues are of minor impact on the phenomenology and of minor concern for the current studies. As there is no reason to expect the hidden sector in nature to be of exactly the form considered here, the aim of this paper is not precision but rather phenomenological and experimental guidance, in search of robust analysis strategies.

II. THE CASE STUDIES

A. Preliminaries

The studies below will all involve decays of a Z' of mass 3.2 TeV to a hidden valley sector. In many models the Z' will already been discovered in its decays to dilepton final states. However, knowledge of its presence and of its mass do not significantly aid in uncovering the hidden valley signal, because of the latter's complexity. In other models, the branching fraction of the Z' to dileptons will be too small, and the Z' will not yet have been identified when the hidden valley signal is sought.

As noted in Sec. I A, signal cross-sections in the 10–100 fb range are consistent with LEP I and LEP II constraints. The cross-section is easily changed by an additional factor of 10, without altering the observable phenomenology in any other way, by adjusting the $U(1)'$ coupling constant g' (see Fig. 5). For simplicity, I will study samples of 1000 events, such as might be obtained in a real LHC

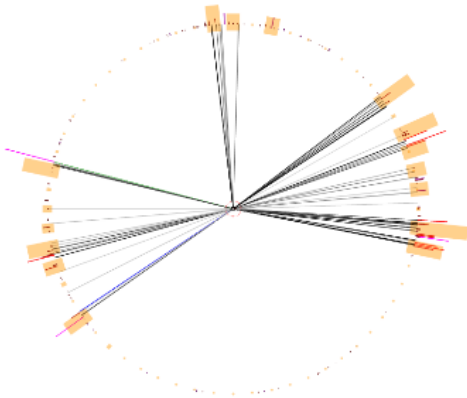


FIG. 7: A schematic view of a typical event from case A1. The view is along the beampipe. Charged tracks are shown in the “tracker”, the central disk in the figure. Since there is no magnetic field in this event display, all tracks with $p_T < 3$ GeV have been removed; grey-level corresponds to p_T , with hardest tracks shown in black. Neutral hadrons and photons are indicated as outward-pointing lines starting at the outer edge of the tracker, and calorimeter energy in azimuthal angular bins of width $2\pi/60$ are shown as bars at the outer edge of the tracker.

analysis. *All plots shown below, except where noted, show results for 1000 simulated signal events.*

The case studies are distinguished by the masses of the v -pions and by whether the π_v^\wedge are stable or decay promptly. In Table I the cases are listed. In addition to the masses and decay settings, the table shows the average multiplicity of visibly-decaying v -pions and some kinematic information: the transverse calorimeter energy \hat{H}_T , the invariant mass M_4 of the four highest- p_T jets, and the average missing transverse momentum (MET, or \cancel{E}_T). The quantities \hat{H}_T and \cancel{E}_T are computed here using scalar and vectorial sums of the p_T of all calorimeter

Case	π_v^\wedge stable?	m_{π_v} (GeV)	R	$\# \pi_v$ decays	\hat{H}_T (GeV)	M_4 (GeV)	\cancel{E}_T (GeV)
A1	Yes	50	368	4.0	667	590	318
A2	Yes	120	883	2.4	765	667	400
A3	Yes	200	1470	1.5	886	770	459
B1	No	50	368	10.3	1650	1427	214
B2	No	120	883	6.1	1835	1562	182
B3	No	200	1470	3.9	2248	1810	145

TABLE I: The case studies, showing the stability of the π_v^\wedge , the mass of the v -pion, the ratio $R = \Lambda_v/\Lambda_{QCD}$, the average number of visible v -pion decays, and the average \hat{H}_T , M_4 , and \cancel{E}_T .

towers,

$$\hat{H}_T \equiv \sum_{towers} |\vec{p}_T| \Theta(|\vec{p}_T| - 5 \text{ GeV}) \Theta(|\eta| - 3) ; \quad (2)$$

$$\cancel{E}_T \equiv \left| \sum_{towers} \vec{p}_T \right|. \quad (3)$$

The calorimeter towers combine the 3-momenta of the various hadrons, electrons, photons *and muons* in 0.1×0.1 bins in pseudorapidity η and azimuthal angle ϕ . For \hat{H}_T I include only towers with $p_T > 5$ GeV and $|\eta| < 3$, as indicated by the Θ functions, to reduce significantly the impact of the underlying event. (However, for a fully realistic study, an H_T variable built from the reconstructed jets might be much more robust; in these models, a variable $H_T^{(jet)}$, defined as the scalar summed p_T of all jets with $p_T > 25$ GeV and $|\eta| < 3$, takes values about 10 percent larger than \hat{H}_T defined above.) Meanwhile M_4 , the invariant mass of the four highest- p_T central jets, is built from jets defined using the midpoint cone algorithm of cone radius 0.4; see Sec. IID and Appendix B below.

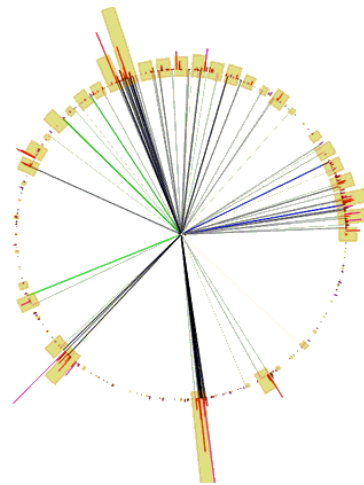


FIG. 8: As in Fig. 7, a schematic view of a typical event from case B1.

Note the obvious progressions in the table. Comparing A1, A2 and A3, one sees the decrease in the multiplicity of v -pions; the same trend appears in B1, B2 and B3. Meanwhile the B cases, with a decaying π_v^\wedge , have roughly triple the number of visibly decaying pions, much higher visible energy, and much less \cancel{E}_T , compared to the A cases for the same v -pion mass. For illustration, event displays of one event each from cases A1, B1 and A3 are given in Figs. 7–9. However the reader should bear in mind that event-to-event fluctuations in appearance are much

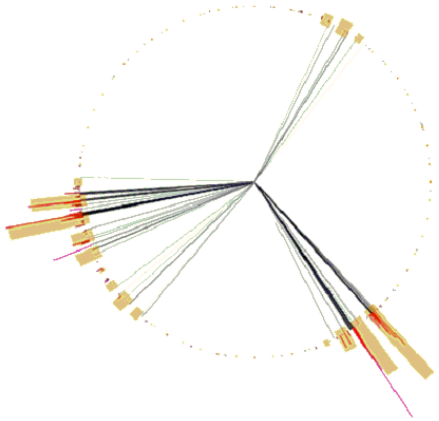


FIG. 9: As in Fig. 7, a schematic view of a typical event from case A3.

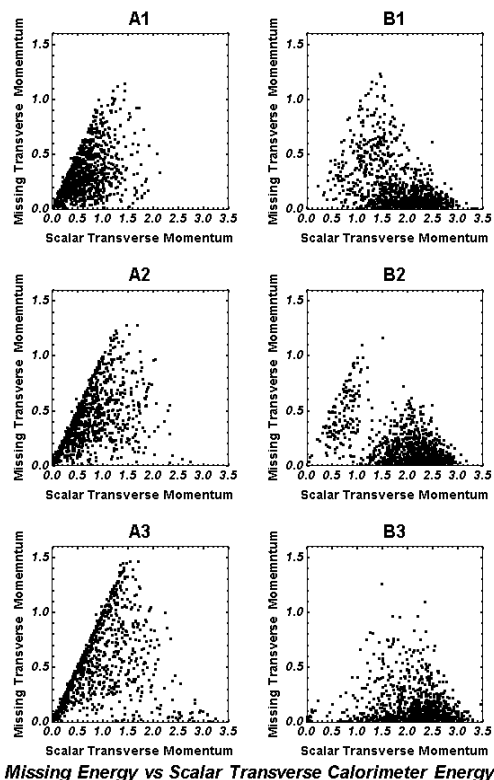


FIG. 10: The distribution of missing transverse momentum (MET) versus \hat{H}_T in TeV. These quantities are defined in Eqs. (2)-(3).

larger here than in most standard model backgrounds or traditional new signals such as gluino production.

Figure 10 shows \hat{H}_T versus \cancel{E}_T for the various cases. The difference between the A cases, where roughly 2/3 of the ν -pions are stable and escape undetected, and the B cases, where the ν -pions all decay promptly and most of the debris from the Z' is observed, is obvious. Occasional ν -baryons (stable and invisible in all present case studies) can provide some \cancel{E}_T even in the B cases. There is additional and sometimes substantial \cancel{E}_T from secondary neutrinos produced in semileptonic decays of b and c quarks and especially in τ decays.

Already from these plots, one sees clearly that *the A cases will have much larger standard model backgrounds than the B cases*. The B cases are more similar to those studied in [16], though with a higher invariant mass, lower rate, and no dilepton resonance. I will show in Sec. IID that they have many reconstructed hard jets. Backgrounds are high-multiplicity QCD events with many b quarks, including $t\bar{t}b\bar{b}$, $b\bar{b}b\bar{b}jj$, $t\bar{t}t\bar{t}$, $t\bar{t}Z$, $t\bar{t}b\bar{b}$, *etc.* These signals tend to be in the few pb range or less, and will be greatly reduced by an \hat{H}_T cut at, say, 800 GeV. The A cases, by contrast, despite their large \cancel{E}_T , are often in the same overall kinematic regime as relatively low-energy standard model processes with a few jets and \cancel{E}_T . These much larger backgrounds include W or Z plus jets (especially heavy flavor), $t\bar{t}$ plus jets, $t\bar{t}W$ or $t\bar{t}Z$, $t\bar{t}b\bar{b}$, *etc.* Cuts on \hat{H}_T and \cancel{E}_T that have high efficiency for the signal will still leave considerable amounts of background behind.

In contrast to standard model backgrounds, triggering should not be a problem for either the A or B cases. Most of the events in this signal will pass the various jet(s) or jet(s)-plus- \cancel{E}_T triggers, with the latter being most efficient for the A cases. Even in the A cases, due to secondary muons, many events will also pass dimuon and muon-plus- \cancel{E}_T triggers; see Appendix A. The trigger will mainly remove unspectacular, low-visible-energy events, which are rare in the B cases and consist of a large minority in the A cases. But the events that fail these triggers are precisely those which would be especially difficult to distinguish from standard model background off-line. Conversely, the events which are most distinctive — with multiple acoplanar high- p_T jets and possibly large \cancel{E}_T — will be among those which will pass the trigger. *For this reason, the effect of the trigger is likely to be relatively minor, compared to the other issues addressed below.*

B. The ν -pions

In these case studies, the Z' decay produces a substantial number of ν -pions, organized into two rather fat ν -jets. All of these ν -pions decay visibly in the B cases, while about a third are visible in the A cases. (Actually the fraction is a bit larger in these QCD-like models, due to ν -isospin violation that, as in QCD, biases the decay of the η_ν toward π_ν^0 s.) The number of visible ν -pions is

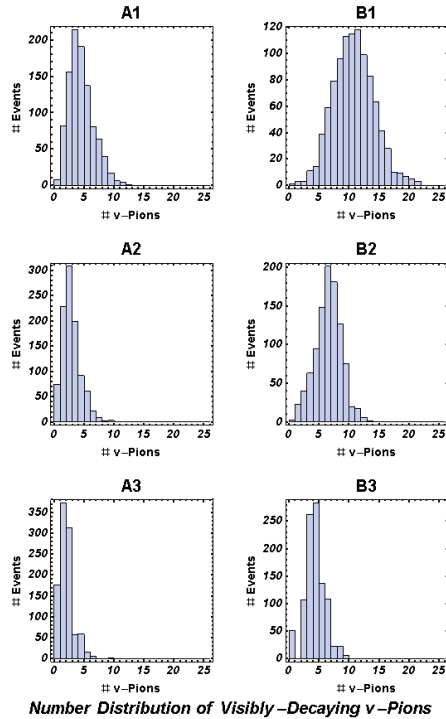


FIG. 11: For the case studies, with 1000 events, the distribution of the number of visibly-decaying v -pions, each decaying to two standard model particles.

shown in Fig. 11. Since the only difference between case B1 and case A1 is the stability of the $\pi_v^{\wedge\vee}$, the distribution of visible v -pions in case B1 equals the distribution of all v -pions, visible and invisible, in case A1. The same applies for B2 and A2, and for B3 and A3.

In Fig. 12 are shown the p_T distributions of the v -pions; notice few have $p_T < 50$ GeV, and most are relativistic. Fig. 13 shows the p_T distribution of the highest- p_T visibly decaying v -pion, which is almost always relativistic, often with a boost factor above 3. This is relevant because *the majority of events have a highly-boosted v -pion whose decay products are separated in η and ϕ by $\Delta R < 0.5$.*; here $\Delta R = \sqrt{(\Delta\eta)^2 + (\Delta\phi)^2}$ as usual. We will see in Sec. IID and Sec. III that the decay products of high- p_T v -pions often are merged into single jets.

As an aside, let us note that the multiplicity distribution and p_T distribution of the v -pions, and the distribution of final-state quark and lepton flavors, is quite different from a thermal distribution, as one would (at least naively) expect in a black hole decay [21, 22], another potential source of high-multiplicity events. Also the events are not in general spherical (see Figs. 7–9) in contrast to expectations for black holes. (See however Sec. IV D of [8].)

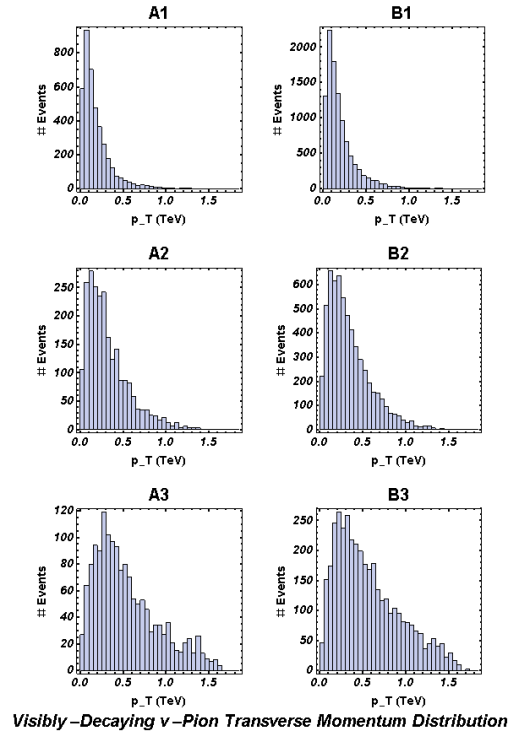


FIG. 12: As in the previous figure, the p_T distribution of the visibly decaying v -pions, in TeV.

C. v -Pion Decay Products

As noted in Sec. IA, the decay rates of the π_v^0 (and the $\pi_v^{\wedge\vee}$ if unstable) to quarks and leptons are roughly proportional to the square of the final-state fermion masses. The fermion mass used should be evaluated at the v -pion mass scale. For simplicity the relative branching ratios to quarks and leptons are taken to be those of a Higgs boson of the same mass as the π_v . Since the π_v does not decay (at tree level) to WW and ZZ , these decay channels are first removed before the branching fractions are computed. In the mass ranges considered here, the unstable v -pions decay mainly to $b\bar{b}$ pairs with a large branching fraction ($\sim 90\%$ for the lighter v -pions), with the remainder going mainly to $\tau^+\tau^-$, $c\bar{c}$ and gluon pairs. The number of final-state (short-distance) standard model particles is simply double the number of visibly-decaying v -pions. Note from Table I that the average multiplicity of final-state partons ranges from 3 in case A3 to 20 in case B1. Also, note in Fig. 11 the wide fluctuations and the long tail, which reaches 42 in case B1 and even in case A3 extends to 12. (However, a fraction of these partons have low transverse momentum, as will be seen below.) The event-to-event fluctuations in the multiplicity of final-state partons are exceptionally high compared to most new-physics signals. This is part of what makes

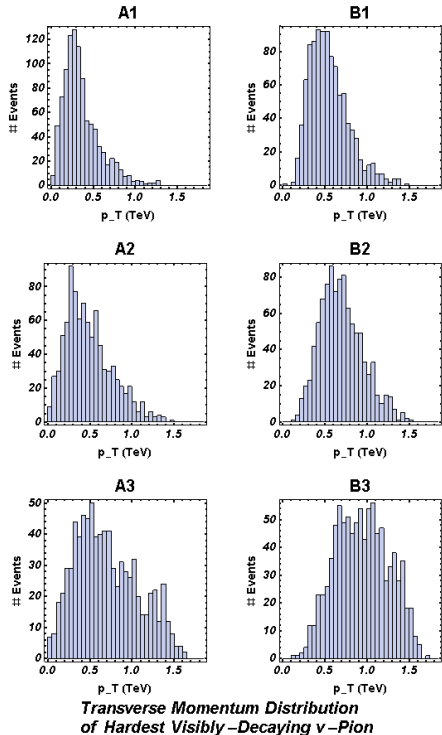


FIG. 13: As in the previous figure, the p_T distribution of the *hardest* (*i.e.*, highest- p_T) visibly decaying v -pion.

this signal challenging.

1. Bottom Quarks and Taus

Most of the final state partons, especially for lighter v -pions where decays to gluons are suppressed, are b quarks and antiquarks. The p_T spectrum of the central ($|\eta| < 2$) b quarks is shown in Fig. 14. For lighter v -pions, the higher multiplicity of b quarks is somewhat compensated by their lower p_T , which makes them less likely to produce jets above kinematic cuts and to decay with detectable vertices. The fraction of bottom quarks that are central ($|\eta| < 2$) and hard ($p_T > 50$ GeV) varies from about 55% for cases A1 and B1 to nearly 85% for cases A3 and B3.

Taus are produced in roughly ten percent of the v -pion decays, and are common in these events. One could imagine that central hadronic taus could be useful in identifying this signal. However, in the present studies, few events have more than two tau leptons, which is not enough to be unusual (given $t\bar{t}$ rates). In addition, one or both tau's will sometimes fail isolation requirements, either because they are too close together (as we will see below) or because of the high multiplicity environment in which they are produced. For this reason, the num-

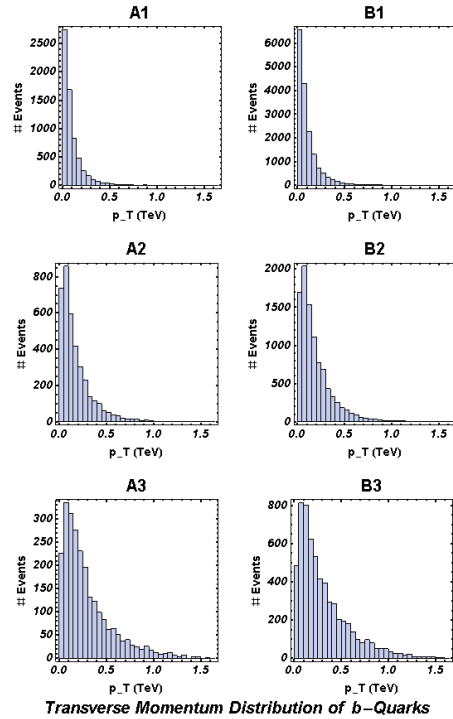


FIG. 14: For the case studies, over 1000 events, the p_T distribution of the daughters (mainly b and \bar{b} quarks) of the v -pions.

ber of taus identified is likely to be too small for it to play a role in extracting the signal. But it should be noted that in other hidden valley models, where the τ -to- b ratio might be enhanced, the role of taus in signal identification might be more important.

2. Secondary Muons and Electrons

In these models, unlike those of [16], electrons and muons do not provide a direct handle for discovering the v -hadrons directly. The branching fraction of the v -pion to muons is tiny (unless the v -pion is lighter than $2m_b$, in which case it will be very long lived). However, because these events have high multiplicity, and because the v -pions decay mainly to b , c and τ , which in turn can produce light leptons (generally non-isolated), it is very

	A1	A2	A3	B1	B2	B3
Fraction of events with 3 or more muons ($p_T > 3$ GeV, $ \eta < 2.5$)	0.09	0.04	0.02	0.46	0.28	0.11

TABLE II: Fraction of events with multiple muons. All cases studies have 1000 events.

common for one or more electron or muon to be produced as a secondary. The presence of these light leptons could assist with reducing backgrounds.

Since the leptons in question are not typically isolated, I focus on muons, which are easier to identify. The numbers of events with three or more muons that have $p_T > 3$ GeV and $|\eta| < 2.5$, with no isolation requirement, are shown in Table II. Note the large number in the B cases. This implies that requiring multiple muons may serve as one of several useful criteria for selecting events for analysis. Unfortunately the number of muons is too small to be of much use in the A cases.

Additional plots related to lepton distributions appear in Appendix A.

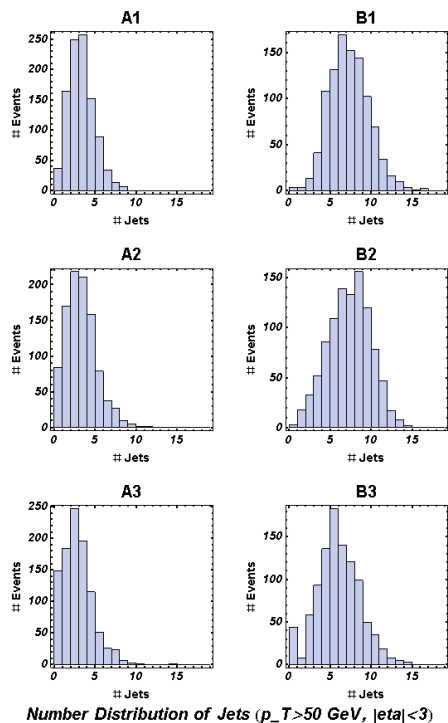


FIG. 15: For the case studies, with 1000 events, the number of jets (formed using the midpoint cone algorithm with cone-size $\Delta R = 0.4$; see text for more details) with $p_T > 50$ GeV and $|\eta| < 3$. The number of jets is considerably smaller than twice the number of visibly-decaying v -pions, Fig. 11.

D. Jets

Typically one characterizes events on the basis of “objects”, where the objects include electrons, muons, photons, hadronic taus, and jets, which may be tagged or untagged. Since the majority of the many jets in the signal are from b 's, one might expect about half of them on average to be tagged, with a few events containing an exceptional number of tags. One might expect these events

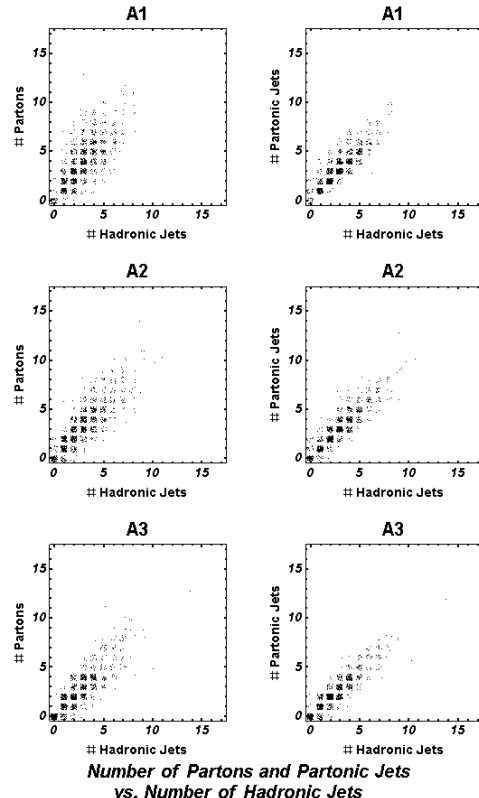


FIG. 16: For the A cases, with 1000 events, the number of partons versus the number of hadronic jets (left plot) and the number of partonic jets versus the number of hadronic jets (right plot). Jets are formed using the midpoint cone algorithm with cone-size $\Delta R = 0.4$; see text for more details. Cuts of $p_T > 50$ GeV and $|\eta| < 3$ are imposed on both partons and jets. One sees that that partonic and hadronic jets are in correspondence, but partons do not correspond as well to jets.

to be the ones that stand out above standard model background.

This expectation is not entirely wrong, but it is also too naive. In particular, *the standard jet-parton correspondence does not work in this signal*. As we will see, the number of well-reconstructed and taggable jets is typically considerably smaller than the number of b quarks. Many jets contain two or more b quarks. While the tagging efficiency may be somewhat higher in such jets, that the number of tagged jets obviously cannot be exceptional if the number of jets itself is not exceptional.

Instead, here and in Sec. II E, I will argue that *treating jets as objects, characterized as either “tagged” or “untagged”, would throw away crucial information needed to separate this signal from background*. A substantial fraction of the jets in this signal are not standard jets, and it appears that this fact may be critical in suppressing backgrounds.

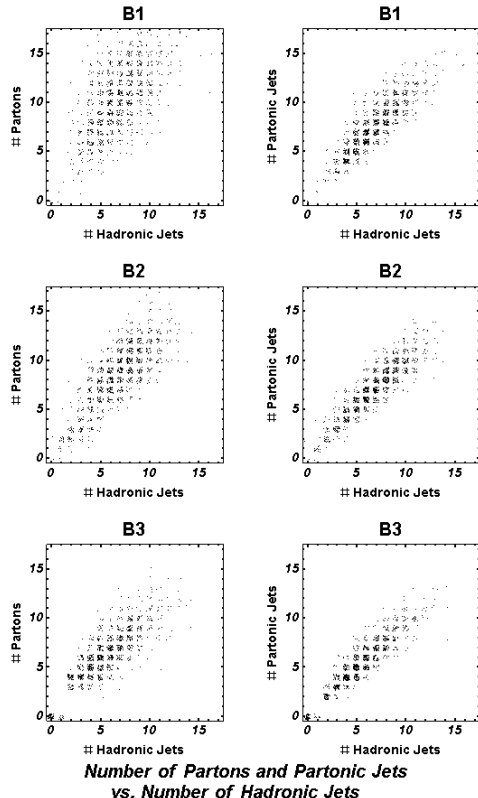


FIG. 17: As in the previous plot, for the B cases.

In the plots shown in the main part of this article, the midpoint-cone jet algorithm is used, with cone size 0.4; more details on the parameters chosen are given in the appendix. Changing parameters, or choosing other algorithms, will change the details, but as argued in Appendix B, will not change the main conclusions of this section. The same may not be said for finding the v -pion resonance, however; see Sec. III.

In Fig. 15 is shown the number distribution of jets per event with $|\eta| < 3$ and $p_T > 50$ GeV. The average number of jets is rather large but not spectacular in the B cases, and not very large in the A cases, which do not even have a substantial tail on the high side. This means one cannot find this signal by simply demanding large numbers of hard jets; in the A cases, a requirement of more than six jets removes most of the signal, and preserves only half of the signal in the B cases. Recall that these signals are in the 10–100 fb range, whereas multi- b backgrounds with 8 or more jets, from $t\bar{t}b\bar{b}$, $t\bar{t}Z$, *etc.*, are in the 1–10 pb range. A hard cut on the number of jets cannot be afforded.

Note also that in all cases the average number of jets is significantly lower than twice the average number of visibly decaying v -pions, shown in Fig. 11. The typical v -pion is not producing two jets. It is important to identify

the reason for this.

Let us first quantify the degree to which the jets do not correspond well to the partons in the event. (In this section, “partons” refers to v -pion daughters, which appear at short distance; it does not refer to partons emerging through subsequent showering.) That there is a mismatch is hardly surprising, given the cluttered nature of these high-multiplicity events. In the left-hand plots of Figs. 16 and 17 are shown the number of partons versus the number of jets; here $p_T > 50$ GeV and $|\eta| < 3$ for both partons and jets. Notice these often differ by as much as a factor of 1.5 to 2. This breakdown of the jet-parton correspondence is natural and indeed has been seen before; it will certainly can occur in $t\bar{t}t\bar{t}$ events, and in events with highly boosted massive particles, such as W ’s, Z ’s, h ’s and t ’s. In this signal, however, it can become extreme.

Fortunately, there remains a close connection between the clustering of hadrons and the clustering of partons. This is partly due to the fact that the final-state quarks are all produced in the decays of the color-singlet v -pions, which limits the radiation of gluons at large angles. In the right-hand plots of Figs. 16 and 17 is shown the relation between *jets of hadrons* and *jets of partons*. Here, the hadrons are clustered according to an algorithm, the partons (*i.e.*, the short-distance v -pion daughters) are clustered according to the *same* algorithm, and the results are compared. Clearly the correspondence of hadronic jets and partonic jets is much closer than that of hadronic jets and partons themselves. In other words, even in this signal, a fixed algorithm applied at the hadron level gives jets that do correspond well to the jets obtained by applying the algorithm at the parton level. It is shown in Appendix B that this result is robust for both cone and k_T algorithms; compare the figures above with Figs. 36 and 37. In particular, although cone and k_T algorithms will find different jets in general, *both algorithms find the same jets in short-distance partons as they do in hadrons*.

Since the partonic jets *are* a good surrogate for the hadronic jets, one can take a short-cut to learn about the failure of the jet-parton correspondence. To determine precisely the number of b quarks in each jet, one should examine the B mesons within the hadronic jets, but this is technically tedious and has subtleties. Instead, one can examine the number of partons collected within partonic jets in various p_T ranges, as shown in Fig. 18. This provides sufficient information to illustrate the key phenomenological points.

Several effects tend to cause multiple partons to be combined into a single jet. First, a high- p_T jet is likely to be a single boosted v -hadron, and so contains two partons. This effect becomes substantial for boost factors above about 3 or 4. This is visible in the right-hand plots of Fig. 18, where it can be seen that jets with $p_T > 200$ GeV have a substantial probability to contain two partons, ranging from 1/3 for the higher-mass v -pions of cases A3 and B3 to 3/4 for the lower-mass v -pions of cases A1 and B1.

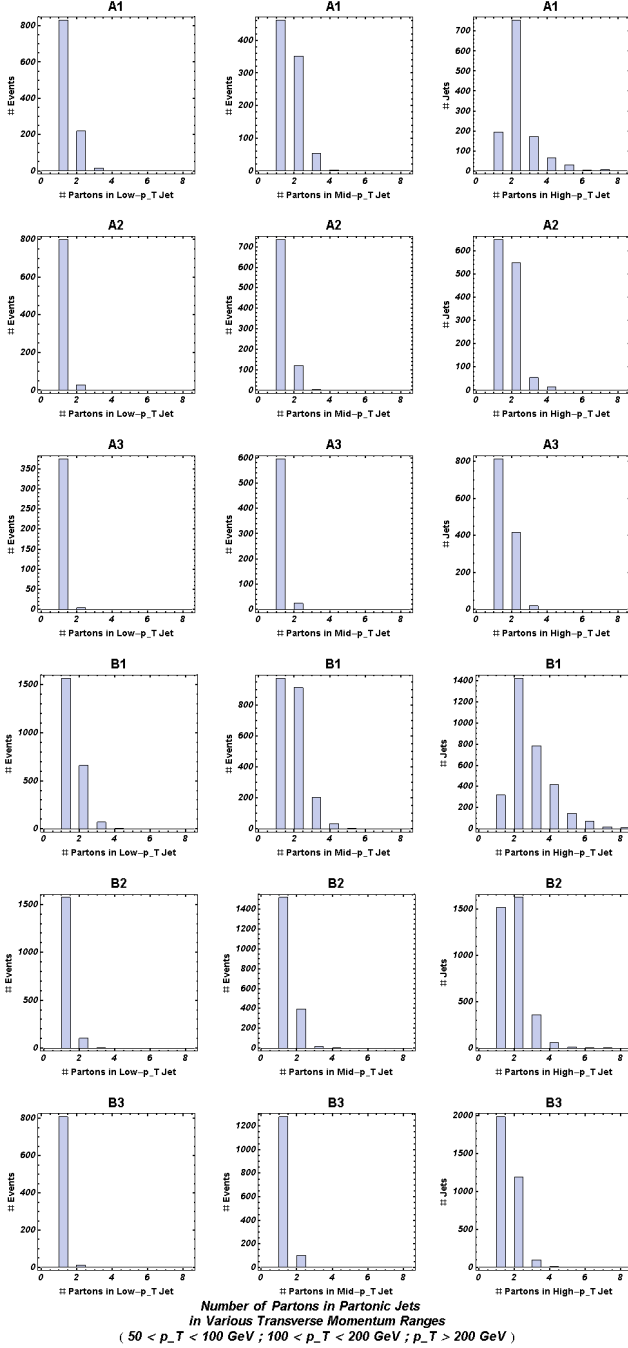


FIG. 18: For the case studies, with 1000 events, the number of partons inside of partonic jets (which correspond well to hadronic jets) for jets with $|\eta| < 3$ and p_T in three ranges: $50 < p_T < 100 \text{ GeV}$ (left plots), $100 < p_T < 200 \text{ GeV}$ (middle plots) and $p_T > 200 \text{ GeV}$ (right plots).

Also, the fat v -hadronic jets from the Z' decay tend to throw multiple v -hadrons into the same region of η and ϕ , so the probability that partons from different v -pions are nearby in η and ϕ is non-negligible. Furthermore, the presence of soft partons from the softer v -pions tends to increase the probability that harder partons will be merged by a jet algorithm. These combined effects can be seen in Fig. 18, which shows that a significant number of jets contain 3 or more partons, even as many as 6 or so, for the cases with lower v -pion mass and consequent higher-multiplicity. Of course the effect is more dramatic for the B cases.

Table III provides some information about b quarks with p_T less than 30 GeV, which often cannot generate a clean jet and are rarely taggable. Recall that the multiplicity distributions in these signals have long tails, so the average number is less than half the maximum. This completely different effect also tends to reduce the number of jets relative to the number of v -pion daughters. Particularly in the case of lighter v -pions, these low- p_T b quarks contribute additional sources of confusion for jet reconstruction, as well as adding tracks and neutrals in the few GeV range but without providing a detectable vertex.

Altogether, this means that the number of jets is significantly less than the number of partons. This is a bit disappointing, as the high multiplicity of partons is a unique and striking feature of the signal. *The mere counting of jets, even with heavy-flavor tags, is unlikely to be enough to separate signal from background, especially in the A cases.*

E. Beyond Jets: Vertexing and Tracking

To identify this signal, it seems likely that tagging of individual jets is not enough. By definition, the number of heavy-flavor-tagged jets cannot be larger than the number of jets. But the number of B mesons can greatly exceed the number of tagged jets, as suggested in Figs. 16 and 17. In other words, although these events do not have an exceptional number of taggable jets, often four or less in the A cases, they do have an unusual number of B mesons. *Thus to distinguish the signal from background, it is essential to detect as many vertices from the B mesons as possible.*

More precisely, *a remarkable feature of this signal is the number of vertices and the distinctive correlations be-*

	A1	A2	A3	B1	B2	B3
Fraction of b quarks with $p_T < 30 \text{ GeV}$	0.27	0.11	0.05	0.25	0.10	0.04
# b quarks per event with $p_T < 30 \text{ GeV}$	1.86	0.44	0.12	4.49	1.02	0.28

TABLE III: Average distributions over 1000 events of soft b quarks.

tween vertices and hadronic jets. Most of the high- p_T jets contain more than one B -meson vertex. This can occur in some standard model backgrounds (through boosted h decays, boosted Z decays, and most commonly through $g \rightarrow b\bar{b}$ splitting) but the probability of having two or more jets with multiple B mesons is low, and the probability of having additional B mesons in the event is also low. (Of course, even a single B may produce a second vertex when its daughter D meson decays, but the kinematic correlations between the parent and daughter vertex are distinctive and different from those of the two B mesons from a π_v decay.) It thus appears that moving beyond “tagged jets” and “untagged jets” as the basic objects of analysis is important for separating signal and background.

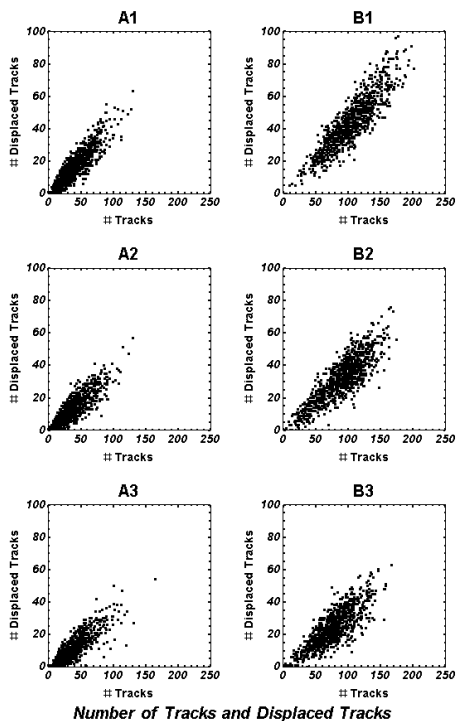


FIG. 19: For the case studies, over 1000 events, the number of displaced tracks versus the total number of tracks. In this plot all tracks have $|\eta| < 2$, $p_T > 2$ GeV, and displacement in three dimensions must exceed 300 microns.

Meanwhile, vertex/jet correlations are not the only non-object-based measure that can be useful. Consider Fig. 19, in which distributions of the number of tracks with $|\eta| < 2$, $p_T > 2$ GeV, versus the number of such tracks with three-dimensional impact parameter > 300 μm , are shown. This is a measure of both the number of B mesons produced and the fraction of tracks that were produced in a B meson decay. In particular, notice that the slope (the fraction of tracks that are displaced) is somewhat larger than in the right-hand plot of Fig. 20,

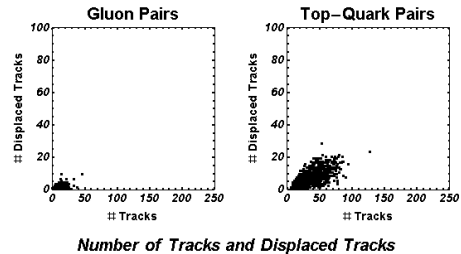


FIG. 20: As for the previous figure, for di-gluon events (left-hand plot) and for $t\bar{t}$ (right-hand plot), generated with PYTHIA, with radiation and the underlying event. In both cases, the samples have $\sqrt{\hat{s}} > 1$ TeV.

which shows $t\bar{t}$ produced at $\sqrt{\hat{s}} \geq 1$ TeV. Thus high-multiplicity heavy-flavor events will have many tracks of which an unusually large fraction will be displaced.

The clustering of the displaced tracks may also be a useful variable, which I have not yet considered. It would be interesting to explore a clustering observable acting upon them.

Presumably, the techniques discussed here would be useful for many other possible new signals. The need to move beyond “tagged” or “untagged” jets is far more general than this particular class of models. It should apply in any signal in which a $b\bar{b}$ pair is produced by a boosted particle, such as a Z or h . (For recent relevant work, see [23].) Obviously the number of tracks and the fraction of tracks displaced are blunt instruments, sensitive to any process with long-lived particles, whether b ’s or something exotic and new. The clustering of tracks and vertices, however, will be variable from signal to signal. For instance, although in the present signal the number of vertices is larger than the number of jets, this inequality need not hold. In signals with novel heavier long-lived particles, which may decay to multiple jets at a displaced point inside the beampipe, a number of jets may share the same vertex, and then the number of vertices per jet may be smaller than one. For example, were case B3 altered so that the lifetime of the $\pi_v^{\wedge\vee}$ were a few picoseconds, and were the dominant decay $\pi_v^{\wedge\vee} \rightarrow gg$, then a single decaying $\pi_v^{\wedge\vee}$ would make two jets, with many displaced tracks, emerging from a single vertex. At the other extreme, there are models in which a large number of light long-lived states are produced, and these can have many vertices. Examples would include cases A1 and B1 with the v-pion mass reduced to 30 GeV and its lifetime extended to a few picoseconds. Then the number of vertices could be very large due to a large v-pion multiplicity, one vertex per v-pion at the point of its decay, and one vertex for each of the daughter B mesons from the v-pion decay. This complex of vertexing issues deserves a thorough exploration by the b -tagging community at the LHC detectors, including LHCb.

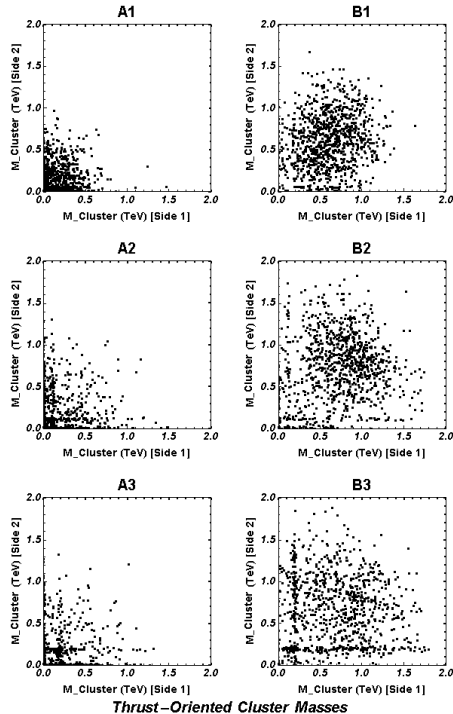


FIG. 21: For the case studies, over 1000 events, the (jet-level) cluster mass in the two hemi-cylinders divided along the transverse thrust axis. Cuts of $p_T > 25$ GeV and $|\eta| < 2$ are imposed on the jets. See cautionary remarks in the text.

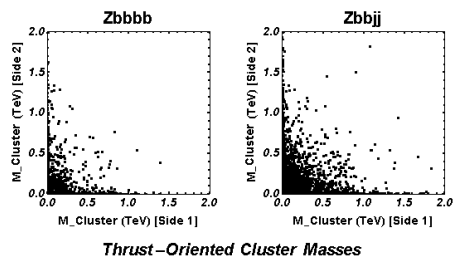


FIG. 22: The (parton-level) cluster mass distribution for the $Zb\bar{b}b\bar{b}$ background ($\sigma \sim 10$ fb, 4200 events shown) and $Zb\bar{b}j\bar{j}$ background ($\sigma \sim 2$ pb, 10000 events shown). See text for more details and cautionary remarks.

F. A Comment on Event-Shape Variables

Here I will briefly explore an event-shape variable for the signals and for two backgrounds. In [16] it was suggested that transverse thrust (defined in the two dimensional plane transverse to the beamline) is a useful variable for separating signal and background. Another variable used was “cluster mass”, obtained by dividing the

cylindrical detector along the plane perpendicular to the transverse thrust axis into two hemicylinders, and computing the invariant mass of all activity within the hemicylinder. To reduce the impact of the underlying event and of initial state radiation, only calorimeter cells satisfying certain p_T and η cuts were used.

In [16], the presence of a dilepton resonance makes even a low signal-to-background ratio acceptable. Here, the signal is smaller, and a much better signal-to-background ratio is needed for the signal to be confirmed (through the methods of the Sec. III). This requires that all cuts have high efficiency for the signal. There are important multi-jet backgrounds (with and without \cancel{E}_T for the A and B cases respectively) that can be disregarded in the case study of [16], but cannot be ignored here.

A proper background study needs to account for many background processes. Below we consider only two, for illustration. These are the ~ 10 fb $Zb\bar{b}b\bar{b}$ process and the ~ 2 pb $Zb\bar{b}j\bar{j}$ process (where j is any non- b quark or gluon, at least two jets have $p_T > 200$ GeV, and the Z decays to neutrinos.) [30] The numbers of events shown in the plots are 4200 for $Zb\bar{b}b\bar{b}$ and 10000 for $Zb\bar{b}j\bar{j}$.

For these two backgrounds, and presumably other multi-jet processes that are the dominant backgrounds remaining after simple cuts, it appears the transverse thrust variable is not helpful. Neither signal nor backgrounds resemble back-to-back di-jets, while neither is spherical, so no cut removes a large fraction of the background without removing most of the signal. But the situation with the cluster mass variable is more promising, as shown in Fig. 21 for signal and in Fig. 22 for the two backgrounds. The cluster masses are here constructed from jets, with $p_T > 25$ GeV and $|\eta| < 2$ to reduce sensitivity to the underlying event and initial state radiation. (This is in contrast to [16], which computed this quantity at parton-level; because of jet merging in the present signal, such an approach would not be reliable here.) The backgrounds (for which jet-parton correspondence is more likely to hold) are shown at parton-level; although this reduces the cluster mass in some events, the effect appears small enough to not affect the general conclusions below.

The larger $Zb\bar{b}j\bar{j}$ background is clearly the more serious problem. It can be reduced if three b tags are required of the events, but at a cost of considerable signal in the A cases. The cluster mass distribution of the signal for the A cases lies underneath the background, and appears not to be useful. By contrast, the B cases (which, as in [16], have few invisible final-state particles) are much more forgiving, as they are for many variables; the cluster invariant mass moves the signal far from the backgrounds shown. A loose cut on this variable, combined with other selection criteria (such as at least three b -tagged jets) should help this signal to stand out.

As an aside, note that the v -pion mass appears visibly in the cluster mass distribution. There is a small but non-negligible probability that a one or both hemicylinders contains only a single v -pion, so that the cluster mass

is just the v -pion mass. However the region in which this is easiest to see lies underneath the background. It seems unlikely that this fact can assist with identifying the signal.

As noted in [16], the cluster mass variable is not sufficiently robust for use in a realistic analysis. Studies for the present paper have shown marked dependence, at the level of 20 percent or more, on the treatment of the underlying event and initial state radiation. The plots above should therefore be treated with caution. They are useful for characterizing differences between signal and background, but a more stable version of this variable should be used in any experimental analysis.

The conclusions in this section are thus preliminary. More robust event-shape variables should be studied, but the cluster mass appears to reduce background in the B cases. However, the B cases are already distinctive in other ways. This variable may be most useful in case B3, where the number of jets is not so extreme as in case B1, but the total invariant mass of the jets in each hemisphere is still very large. On the other hand, this particular variable may not be so useful in the A cases, so a different event-shape variable must be sought.

III. CLINCHING THE CASE: DETECTING THE V -PION RESONANCE

I have discussed a number of features of the signal which make its phenomenology atypical. Despite the unusual features of the signal outlined above, they are not obviously sufficient to allow for easy separation of signal from background, if the signal cross-section is indeed 10-100 fb. The standard model backgrounds are large and variegated, consisting of tails of distributions from a number of different processes. A complete and convincing study will be difficult with present tools. In any case, it seems unlikely that the backgrounds can be understood well enough from data to allow a counting experiment, especially in the A cases, where the number of jets, tracks, vertices, *etc.* is not so large.

Instead, it seems likely that a different strategy is needed. Given the unusual features of the signal discussed above, one might apply loose cuts on these features that have high efficiency for the signal. (For instance, one could require substantial \cancel{E}_T and/or \cancel{H}_T , several jets with at least three tagged, indications of many displaced tracks and vertices, *etc.*) The standard model background surviving the cuts would not be calculable or easily measured, so the signal-to-background ratio would not be well-known. But within this enriched sample, one could then search for the key kinematic feature of the signal – the v -pion resonance – which if observed would confirm that new physics is present.

Simply plotting dijet invariant masses, where the jets are selected at random, cannot reveal the v -pion resonance. The huge combinatoric background, the fact that many jets contain multiple b -quarks, and relatively poor

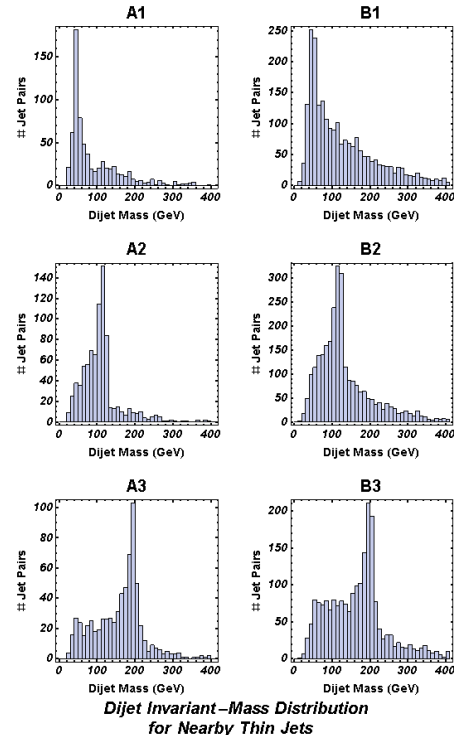


FIG. 23: For the case studies, over 1000 events, the distribution of dijet invariant mass for pairs of thin jets ($m_j < 0.15p_T$, $p_T > 25$ GeV, $|\eta| < 3$) that are nearby ($\Delta R < 1.2$).

resolution for jet momentum and energy would eliminate any signal.

Since many v -pions are boosted, they often form a single jet, or dissociate into two nearby jets. I will use these facts below in studying both dijet invariant mass m_{jj} and single-jet invariant mass m_j below. Clearly both might be used; there is no sharp dividing line between them in any case, since any jet algorithm separates the two in an arbitrary way. (Approaches that avoid this division are under study [25].) It appears that it is important to choose one's jets carefully.

A proper study of these variables would account for the finite resolution in jet energy, momentum and mass. There are many issues here, some beyond the scope of a theoretical investigation. In this study I will include decays, showering and hadronization but will work only with a perfect calorimeter – perfect except for its granularity of 0.1×0.1 in η and ϕ and its limited pseudorapidity coverage — and will show that substantial challenges arise even before realistic detector issues are accounted for.

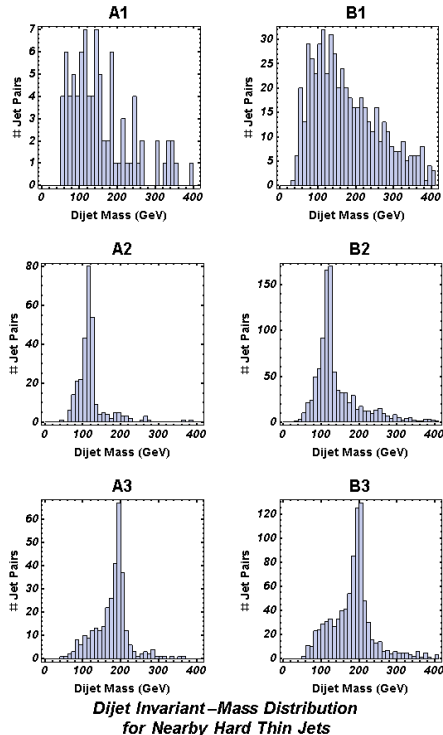


FIG. 24: As in the previous figure, except that the jets have $p_T > 100$ GeV and pairs are within $\Delta R = 0.9$ of one another.

A. Dijet masses

Let us begin with dijet invariant mass. A plot of the invariant masses of all pairs of jets above a certain p_T cut would suffer from an overwhelming combinatoric background, because of the high jet multiplicity. Instead, it is best to use the fact that high-energy Z' decays provide a substantial boost to many of the v -hadrons, as we saw in Sec. II. Most high- p_T jets are either single v -hadrons, whose decay products have merged, or they represent a single quark produced by the decay of a v -hadron whose other decay product will lie close by in ΔR . The difference between these two cases is (on average) that the former class of jets will have a single-jet invariant mass m_j larger than the latter class. In particular, we will distinguish between “thin” and “thick” jets, thin jets being those with $m_j < 0.15p_T$, and thick jets being those with $m_j > 0.15p_T$. (This terminology has been introduced in [25].) By selecting thin jets with high p_T , and plotting the dijet invariant mass of pairs of such jets with ΔR not large, one might hope to significantly reduce the combinatoric background. (This same method works for finding W bosons in high-energy $t\bar{t}$ events.)

In Fig. 23 is shown a plot of dijet masses for cone jets (defined as described in Sec. IID and in Appendix B.) I demand that both jets are thin and have $p_T > 25$

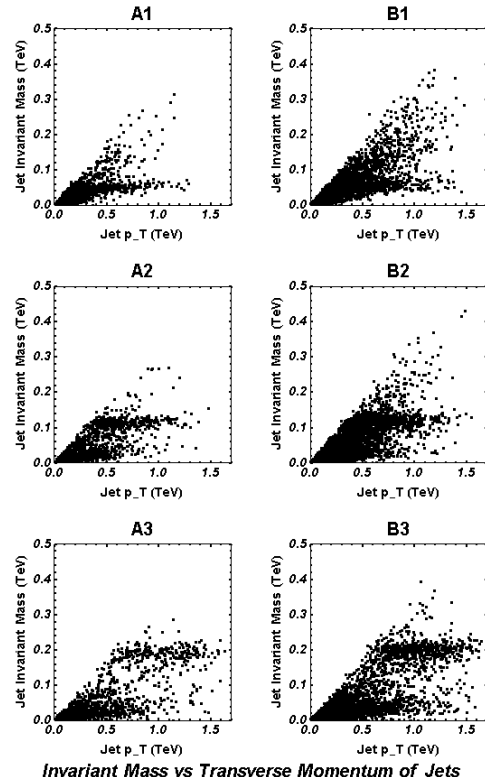


FIG. 25: For jets with $p_T > 20$ GeV, the distribution of m_j versus p_T , in TeV.

GeV and $|\eta| < 3$, and require that the two jets have $\Delta R < 1.2$. In Fig. 24 is shown a similar plot with lower statistics but lower background, using $p_T > 100$ GeV and $\Delta R < 0.9$. Either approach is a challenge for cases A1 and B1, which is not surprising, since reconstruction of a 50 GeV resonance using jets is no easy task. As can be seen from the plots, the number of v -pions reconstructed is disappointingly low; recall there are thousands in the data (see Table I.) Smearing and mismeasurements, not included here, will only make matters worse. It would appear that dijet invariant mass is not a particularly good variable for reconstructing the v -pion resonance.

B. Single jet masses

Now let us turn to single jet invariant mass m_j . In Fig. 25 m_j versus p_T is shown for all jets in these events with $|\eta| < 3$. The same is shown in Fig. 26 for the highest- p_T jet in each event. In both classes of plots, a band of jets with invariant mass near to the v -pion mass is clearly seen. However, this information is not entirely observable. High p_T QCD jets will often develop an invariant mass of order 15 percent of their p_T just from the emission of a moderate- k_T gluon that lies out-

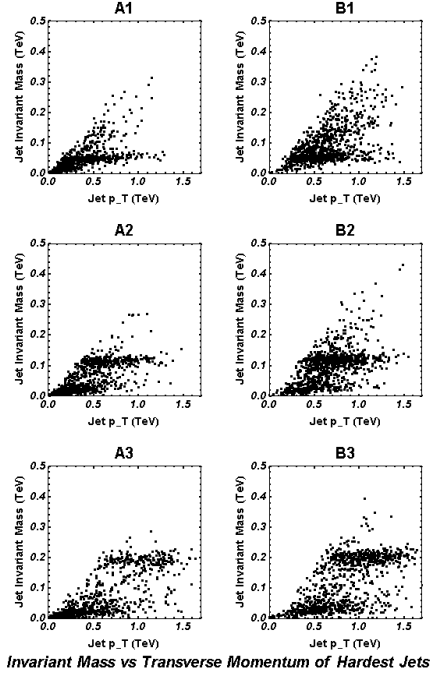


FIG. 26: For the highest- p_T jet in each event, the distribution of m_j versus p_T , in TeV.

side the parton-shower approximation used in PYTHIA’s simulation of jets. Also, jets which are too narrow will not have a well-measured invariant mass, for various detector-related reasons. One might therefore wisely exclude from analysis any jet whose mass is less than, say, 15 or 20 percent of its p_T , thus excluding the hardest jets. Refinements of this measurement deserve more attention than can be given here. However, some preliminary indications are presented in Fig. 27, where the single jet invariant mass of all jets with $p_T > 100$ GeV is shown on the left, and the same with the additional condition that the jet be “thick”, $m_j > 0.15p_T$, is shown in the second-to-left column. Clearly the additional condition has the advantage of removing many ordinary isolated jets, reducing the QCD continuum that peaks at low mass, and allowing the signal to stand out more clearly. This more refined measure of invariant mass is shown again in the right-hand plots of Fig. 27, for the highest- p_T and second-highest- p_T jet in each event. Interestingly, in case B1 — the case with highest multiplicity, where the highest- p_T jet often is a merging of more than two partons (Fig. 18) — the second-highest- p_T jet shows the v -pion mass more clearly. The correlation between the masses of the two highest jets can also be a useful variable; a scatter plot of the masses of the two highest- p_T jets (if both are central and thick) is shown in Fig. 28. Note that in case B1 the high multiplicity tends to spread out the peak, whereas in case A3 the peak is almost invisible due to low statis-

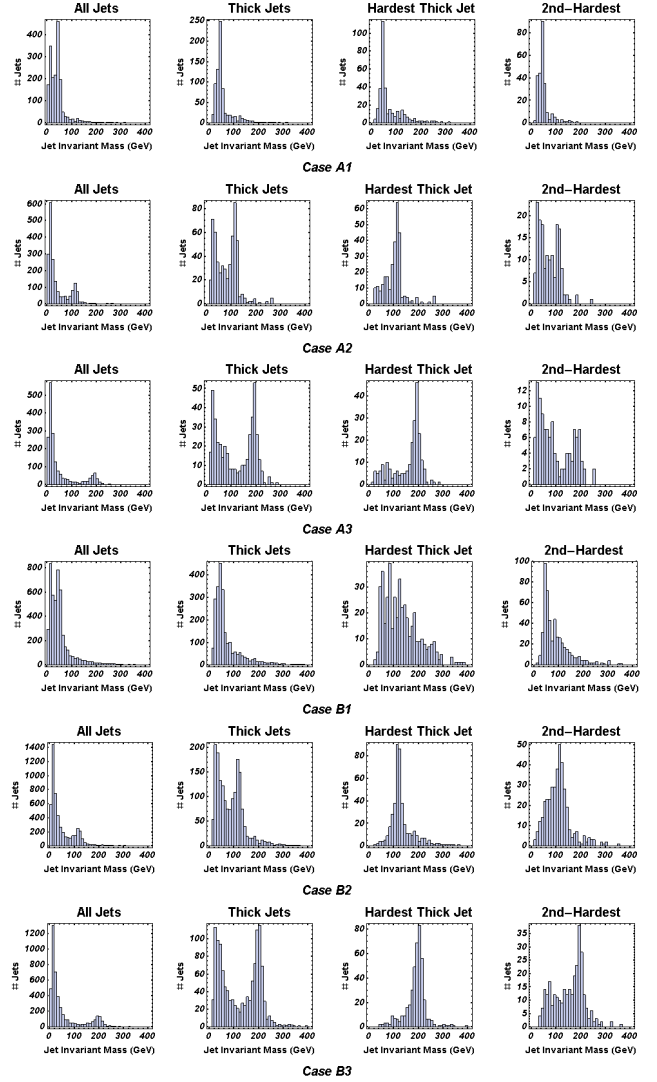


FIG. 27: For the case studies, over 1000 events, the plots, from left to right, show (a) the distribution of single jet invariant mass m_j for jets with $p_T > 100$ GeV and $|\eta| < 3$; (b) the same, with the additional condition that the jets be “thick”, namely $m_j/p_T > 0.15$; (c) the invariant mass of the highest- p_T jet (if $p_T > 100$ GeV, $|\eta| < 3$, and $m_j/p_T > 0.15$), and (d) the same as the previous plot but for the second-highest- p_T jet (with the same cuts.)

tics, but for the other cases this plot can help reveal the resonance.

The fact that the single-jet invariant mass is a good observable in all 6 cases is a simple consequence of the fact that relatively light particles are being produced with a large boost, through the decay of a heavy Z' . (Clearly the same strategy will not work for v -pions produced in decays of lighter particles, such as Higgs bosons [1, 14] or supersymmetric particles [15].) There are important and little-studied backgrounds from all-hadronic decays

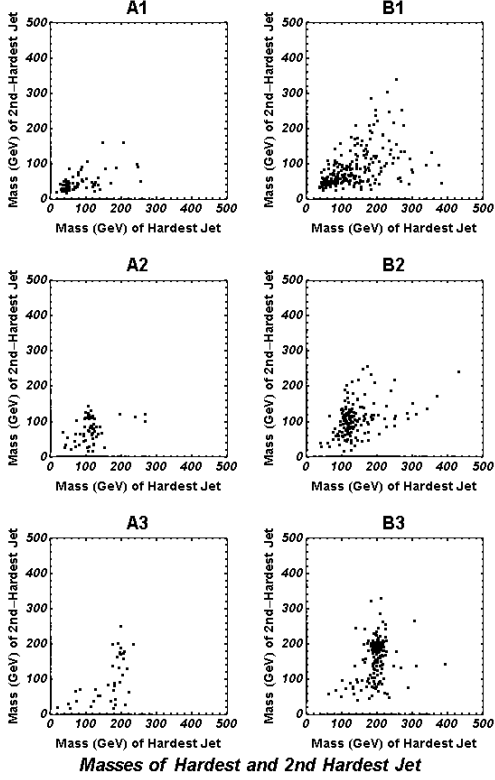


FIG. 28: Jet-invariant mass (in GeV) for the highest and second-highest p_T jets in each event; jets are required to have $p_T > 100$ GeV, $m_j > 0.15p_T$, and $|\eta| < 3$.

of boosted W 's, Z 's, and t 's, which are produced with an enormous rate. These will swamp any new resonance unless events are first selected with the unusual features of this signal. Should the v -pion mass lie close to 80-90 GeV or to 170 GeV, the difficulties will be very much greater. We must hope nature does not choose this scenario, or at least provides a large cross-section in return.

C. Some Improvement Using Fatter Jets

We have seen that single jet invariant mass reconstructs more v -pions than does dijet invariant mass. By widening the jet cone, one might hope to reconstruct even more. Here I will explore increasing the cone radius from 0.4 to 0.7, and will show some increase in efficiency.

Comparing Fig. 29 to Fig. 25, we see that a larger fraction of the jets of radius 0.7 are single v -pions, compared to those of radius 0.4. This is very clear in the left-hand plots of Fig. 30; whereas the thickness criterion (the cut in m_j/p_T) is essential to remove random jets in the signal in Fig. 27, it is less essential, but still effective, with the larger cone size. Comparison of Fig. 30 with Fig. 27, and

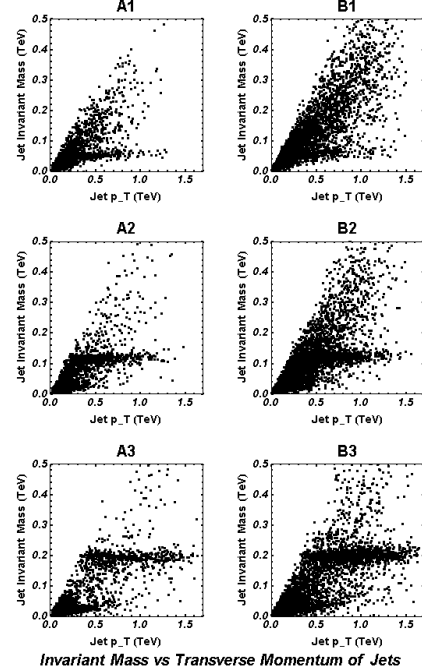


FIG. 29: As in Fig. 25, but with cone size 0.7 instead 0.4; for jets with $p_T > 20$ GeV, the distribution of m_j versus p_T , in TeV.

of Fig. 31 with Fig. 28, shows that the larger cone size generally allows a marked improvement in both efficiency and resolution, for both the hardest and second-hardest jet in the event.

The one interesting exception, among the case studies, is case B1. Here the number of partons in the final state is so large that confusion background dominates. Most high- p_T jets contain multiple b quarks, and the hardest jets tend to contain more than 2, a tendency already visible in Fig. 18. With a cone size of 0.4, rather few of the high- p_T jets are single v -pions, and a larger cone-size makes this problem worse. It appears it is best in this case to work with the jets of radius 0.7 that do not have the highest p_T , and even then the background from random jets in the signal is rather large (see Fig. 30, fourth line, second plot from left). Background from standard model processes would be very problematic except for the fact that case B1 is also the easiest case to separate from the standard model using other methods. This case has the highest multiplicity of jets (~ 7) and vertices (~ 20), the highest multiplicity of secondary muons (~ 3), the most tracks (~ 100) and displaced tracks (~ 50), very high \hat{H}_T (~ 1.6 TeV), and a striking event shape (sum of the two cluster masses ~ 1.2 TeV). Perhaps this signal can even be identified in a counting experiment, where the standard model backgrounds can be estimated from the data by looking at event samples that share some but not all of these striking features. It is conceivable that

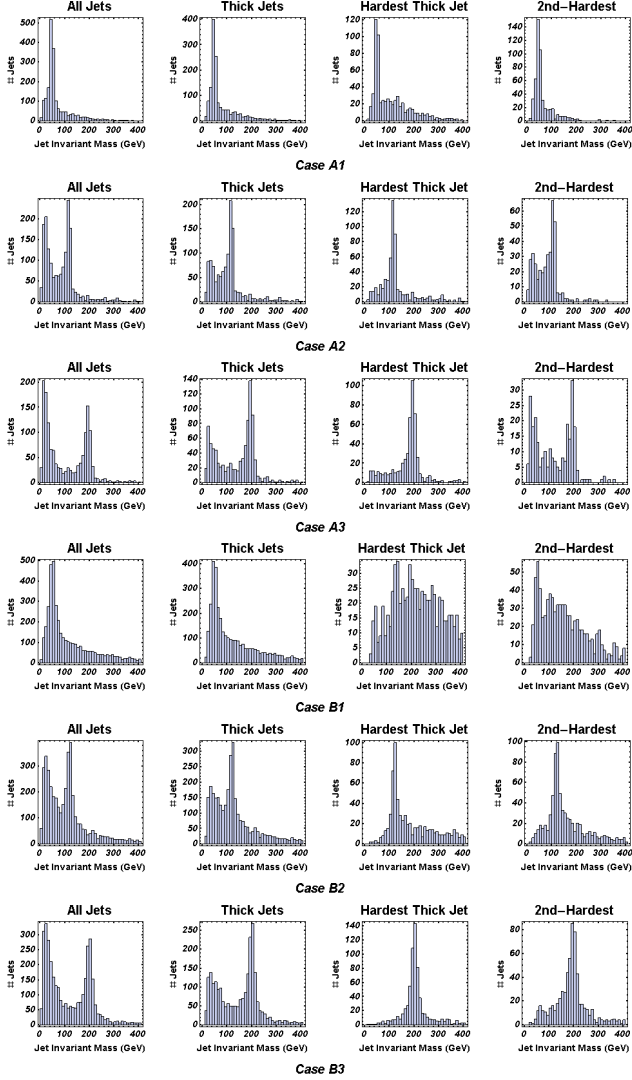


FIG. 30: As in Fig. 27, but with cone size 0.7 instead 0.4; from left to right, (a) the mass m_j of jets with $p_T > 100$ GeV and $|\eta| < 3$; (b) the same but with $m_j/p_T > 0.15$; (c) m_j for the highest- p_T jet with jets with $p_T > 100$ GeV, $|\eta| < 3$ and $m_j/p_T > 0.15$; and (d), the same but for the second-highest- p_T jet.

the v -pion resonance can be better identified with a more sophisticated variable than single jet mass, looking more carefully at the substructure of the jets. (It is even possible that, with so many v -pions per event, and with a bit more statistics than available here, the v -pion can be discovered through its rare tree-level decay to muon pairs or its loop-induced decay to photon pairs.) More generally, it is important to study further how best to look for resonances in very-high-multiplicity signals, such as case B1.

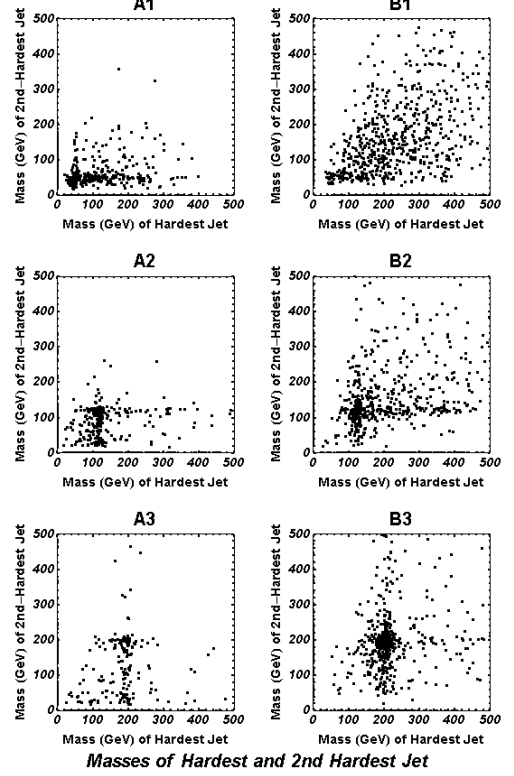


FIG. 31: As in Fig. 28, but with cone size 0.7 instead 0.4; jet-invariant mass (in GeV) for the highest and second-highest p_T jets in each event, where jets are required to have $p_T > 100$ GeV, $m_j > 0.15p_T$, and $|\eta| < 3$.

D. Comments

I have given evidence that single jet mass, using a larger cone size than typically used for jets at the LHC, is the variable to use in searching for the v -pion resonance. Why are the fatter jets a better choice? If a single boosted v -pion has a boost factor greater than 6, it will typically form a single *thin* jet. Thus, thick jets arise from v -pions with a boost below 6, whose daughters typically have an opening angle of order 0.3 or larger. This is why, if a thickness criterion is applied, jets of radius 0.7 have a much higher efficiency for containing a single v -pion than jets of radius 0.4.

These conclusions are somewhat suspect, and the plots above unrealistic, because no energy smearing or magnetic field were included in the simulation of the calorimeter. A more serious study is needed, using a more complete detector simulation. Several remarks are in order.

It will be of considerable interest to learn the jet-mass resolution of the LHC detectors. This information should be available in the early data from studies of W bosons and t quarks in boosted $t\bar{t}$ events. It will also be interesting to see plots of the QCD continuum background to

jet-mass measurements.

Since angular resolution is essential for jet mass measurements, the curvature of tracks due to the magnetic field should be removed. Clearly the use of something like “particle flow” — combining angular information from the tracker as well as the electromagnetic and hadronic calorimeters — should significantly aid in improving the resolution on jet mass.

An additional handle for reducing backgrounds to boosted v -pions may lie in detecting the substructure within the jet, such as recently considered in [23]. This is easiest to do with clustering algorithms such as the k_T algorithm, and using tracking as well as calorimetry. In fact, for the most energetic v -pions, whose daughters have the lowest angular separation, the granularity of the calorimeter, especially its hadronic component, will badly degrade jet-mass resolution. In this case tracking is crucial (see for example [26].) By studying the locations of the highest- p_T tracks, one may be able to significantly improve angular resolution on the substructure of the jet, and improve the invariant mass measurement. These issues deserve much more attention and will be explored elsewhere [25].

IV. CONCLUSION

In this paper I have investigated the phenomenology of a large class of hidden valley models, illustrated by six case studies within a particular model, but intended to apply in a much broader context. The models present a single new narrow resonance (more precisely, in the particular case studied, a triplet of nearly degenerate resonances $\pi_v^0, \pi_v^\wedge, \pi_v^\vee$) that decays promptly, and predominantly to heavy flavor. Importantly, there is no measurable rate for decay to $\mu^+\mu^-$ or e^+e^- . In this sense this class is largely orthogonal to the large class studied in [16]. In production mechanisms (Z' decay) that lead to high-multiplicity heavy-flavor final states, the phenomenology is very different from that of most supersymmetry, technicolor, Randall-Sundrum, or little Higgs models that have so often been studied.

The six case studies were divided into the A cases (where the π_v^\wedge, π_v^\vee are invisible and stable) and the B cases (where all three types of π_v decay promptly). The main results were the following:

- Missing energy and total transverse energy are useful global variables.
 - In the A cases, \cancel{E}_T and \hat{H}_T are of the same order, many hundreds of GeV for 50 GeV v -pions and closer to a TeV for 200 GeV v -pions.
 - In the B cases, the \cancel{E}_T is much smaller and the \hat{H}_T is in the 1.5–2.5 TeV range.
- Multiplicities of v -hadrons, and their daughter standard model partons (mostly bottom quarks), are very large.

- In the A cases, the number of v -hadron daughters ranges from an average of 3 with a tail to 12 (for heavy v -pions) to an average of 8 with a tail to 24 (for lighter v -pions).
- In the B cases, the number of v -hadron daughters ranges from an average of 8 with a tail to 20 (for heavy v -pions) to an average of 20 with a tail to 42 (for lighter v -pions).
- However the multiplicity of jets is somewhat smaller, because jets often contain multiple v -hadron daughters; this is due to the high boost and high concentration of the v -pions.
 - In the A cases, this effect is especially important, because by reducing the number of hard jets it leaves the signal with larger standard model backgrounds.
 - In the B cases, the effect is more pronounced, but the resulting multiplicity of jets is still large compared to most standard model processes.
- In the A cases, counting of heavy-flavor-tagged jets appears insufficient for separating signal from background, because the multiplicity of jets is too low. The situation in the B cases is somewhat more promising.
- The signal is particularly unusual in the numbers of vertices, of tracks, and of displaced tracks, and the clustering of and correlations among jets, tracks and vertices. These features may be useful in separating signal from pbackground.
- Other observables, including event-shape variables (particularly one similar to the $M_{cluster}$ variable of [16]) and numbers of secondary muons, might serve as additional tools for event selection, though their utility needs more study. They may not be helpful in the A cases, and they may not be needed in the B cases.
- If the unusual features of the signal can be used to obtain a sample with a reasonable signal-to-background ratio, an attempt can be made to find the v -pion resonance.
 - Because of combinatorics, a naive approach to dijet masses cannot work.
 - Since many v -pions are boosted, it is better to consider dijet masses of jets which are close in η and ϕ , or single-jet masses of individual jets which are “thick” (have a large mass-to- p_T ratio.)
 - Single-jet mass for a relatively fat jet definition seems to be an observable with a high efficiency for the signal. Here $R = 0.7$ cone-jets were shown to be better than those with

$R = 0.4$, but a thorough study of the best jet radius was not carried out, nor were other algorithms carefully considered. More work remains to optimize this measurement [25].

- Correlations between the single-jet mass of the highest- and second-highest- p_T jets may be useful in reducing background.
- With extreme multiplicity, as in case B1, jet mass for high- p_T jets is less useful, because too many of these jets contain more than a single v -pion. An alternative observable is not yet known, but also such signals are particularly spectacular, with low standard model backgrounds, and a discovery claim might not require reconstruction of the resonance.
- It is possible but rather unlikely that multiplicities and event rates will be high enough to allow reconstruction of the π_v resonance through the rare decays $\pi_v \rightarrow \mu^+ \mu^-$ or $\pi_v \rightarrow \gamma\gamma$.

In all cases, the phenomenological issues that arise are somewhat unusual, and need to be explored further in more fully realistic studies. Generating relevant and realistic background samples for these unusual signals represents a substantial challenge.

I should again emphasize that the issues and observables discussed in this paper are not limited to these specific models, but will apply more broadly. In a number of classes of hidden valley models, new resonances that decay to heavy flavor are produced in high-multiplicity environments, sometimes with a substantial boost. This can also happen in models beyond the hidden valley scenario.

Conversely, it is important to stress that this particular class of models is special, and relatively easy, in that there is only one v -hadron resonance to be found. In many other models, there will be multiple v -hadrons of different masses, and so the resonance signal just described will be spread out among several resonances, making it harder to extract. One may still hope, however, for an enhancement in jet and dijet masses that will be inconsistent with Standard Model background. And some models are even easier to find, as in the example [1] studied phenomenologically in [16], because of the presence of electron-pair and muon-pair resonances. These may easily be seen above background even with a rather impure sample of hidden valley events.

Several other classes of hidden valley models with distinct phenomenology from those studied here and in [16] remain to be investigated. To examine these in detail requires a significant extension of the current Monte Carlo simulation package. An initial extension is now complete [18]. Preliminary results on some models, with their own unusual signals, will be presented soon [27].

I thank G. Ciapetti, A. De Roeck, C. Dionisi, S.D. Ellis, S. Giagu, T. Han, J.W. Huston, P. Loch, H.J. Lu-

batti, G.P. Salam, Z. Si, C.K. Vermilion, J.R. Walsh and K.M. Zurek for useful discussions. I am especially indebted to S. Mrenna and P.Z. Skands for advice and assistance in the writing of the HVMC 0.5 Monte Carlo package. This work was supported in part by Department of Energy grant DE-FG02-96ER40956.

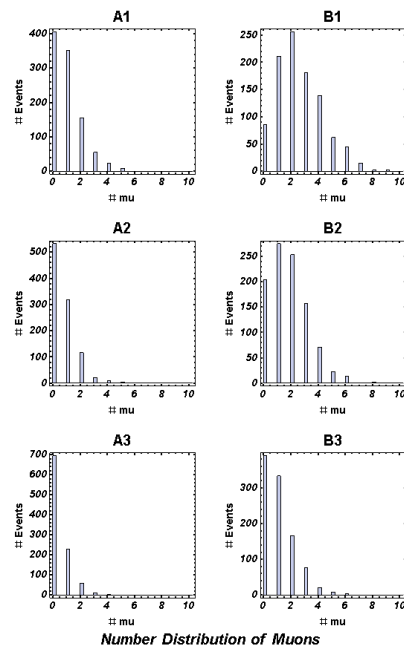


FIG. 32: The distribution of the number of secondary muons.

APPENDIX A: OBSERVATIONS CONCERNING LEPTONS

Plots of the number of central prompt or semi-prompt (appearing within the beampipe) muons, with $p_T > 3$ GeV and $|\eta| < 2$, are shown in Fig. 32, and their p_T distributions are shown in Fig. 33. No isolation criteria are imposed.

APPENDIX B: CHECKING THE CORRESPONDENCE OF HADRONIC JETS AND PARTONIC JETS

Here I will show more carefully that the partonic and hadronic jets, constructed with a reasonable algorithm, do correspond, as claimed in the main text.

The jet algorithms used in this study are shown in Table IV. All studies use the multi-algorithm software SpartyJet of [28], which includes the FastJet k_T algorithm [29]. In the plots within the main text, the midpoint merging version of the cone algorithm was used, with

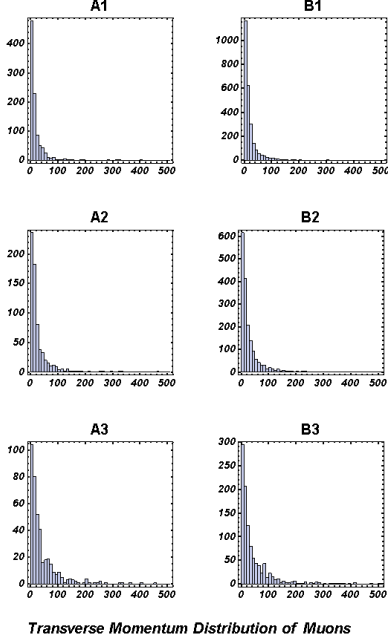


FIG. 33: The p_T distribution of the secondary muons.

cone size $R = 0.4$. In this appendix, a cone of $R = 0.7$ is also used, along with the k_T algorithm with the R parameter set to give k_T jets of radius approximately 0.4 and 0.7.

First, let us check the correspondance between hadronic jets and parton jets. One may confirm that the p_T of the highest- p_T partonic jet matches with the p_T of the highest- p_T hadronic jet; this is shown in Fig. 34. The pseudorapidities match as well. Nor is this an accident limited to the highest- p_T jet; the same figure for the second-highest p_T jet shows that the strong correlation between the hadronic and partonic jets persists.

Now I turn to the k_T algorithm. As with the cone algorithm we see, in Figs. 36 and 37, a failure of the cor-

Midpoint Cone Algorithm			
cone radius	seed threshold	search cone area fraction	merge fraction
0.4	1 GeV	0.25	0.75
0.7	1 GeV	0.25	0.75
FastJet k_T Algorithm			
R parameter	minimum cell p_T	d_{cut}	
0.52	5 GeV	$(5 \text{ GeV})^2$	
0.91	5 GeV	$(5 \text{ GeV})^2$	

TABLE IV: The parameters used in the cone and k_T algorithms used in this study.

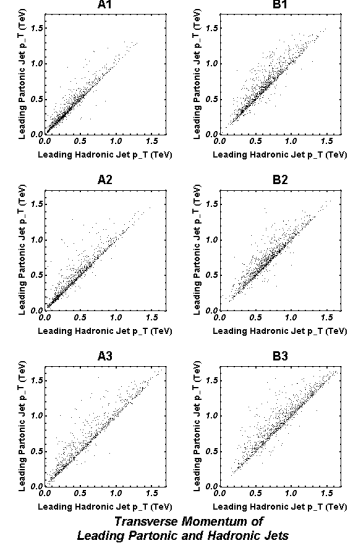


FIG. 34: Correlation between the p_T of the highest- p_T partonic jet and the p_T of the highest- p_T hadronic jet, constructed using the midpoint cone algorithm with $R = 0.4$ (see Table IV.)

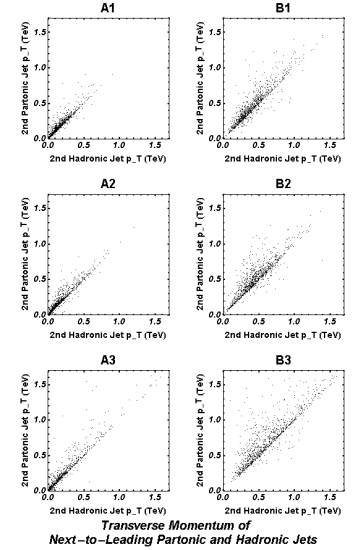


FIG. 35: As in the previous plot, for the second-highest- p_T partonic and hadronic jets.

respondence of partons to hadronic jets, and better agreement between partonic jets and hadronic jets. Figures 38 and 39 further confirm the quantitative correspondence of the partonic and hadronic jets. Thus the cone and k_T algorithms both allow reconstruction of the partonic jets using hadronic jets.

These studies have been repeated for jets with larger settings of the cone size or R parameter (0.7 and 1.0 for cone jets). The correspondence of partonic and hadronic jets continues to hold firm.

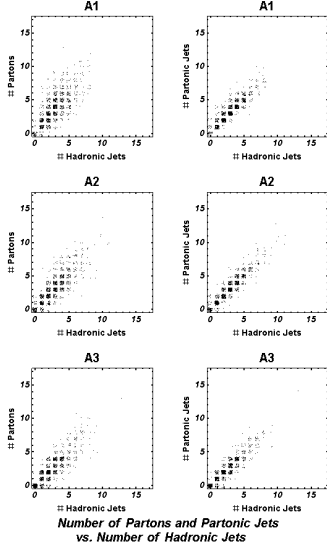


FIG. 36: As in Fig. 16, for the k_T algorithm with R parameter 0.52 (see Table IV.)

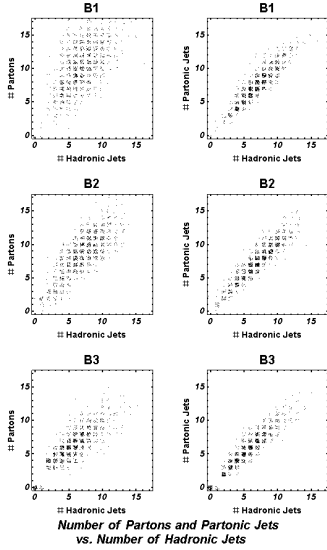


FIG. 37: As in Fig. 17, for the k_T algorithm with R parameter 0.52 (see Table IV.)

-
- [1] M. J. Strassler and K. M. Zurek, Phys. Lett. B **651**, 374 (2007) [arXiv:hep-ph/0604261].
- [2] Z. Chacko, H. S. Goh and R. Harnik, Phys. Rev. Lett. **96**, 231802 (2006) [arXiv:hep-ph/0506256].
- [3] G. Burdman, Z. Chacko, H. S. Goh and R. Harnik, JHEP **0702**, 009 (2007) [arXiv:hep-ph/0609152].
- [4] J. Kang, M. A. Luty and S. Nasri, arXiv:hep-ph/0611322; J. Kang and M. A. Luty, arXiv:0805.4642 [hep-ph].
- [5] H. Georgi, Phys. Rev. Lett. **98**, 221601 (2007) [arXiv:hep-ph/0703260].
- [6] P. J. Fox, A. Rajaraman and Y. Shirman, Phys. Rev. D **76**, 075004 (2007) [arXiv:0705.3092 [hep-ph]].

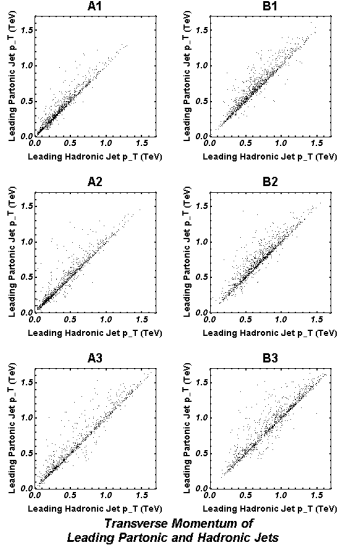


FIG. 38: As in Fig. 34, for the k_T algorithm with R parameter 0.52 (see Table IV.)

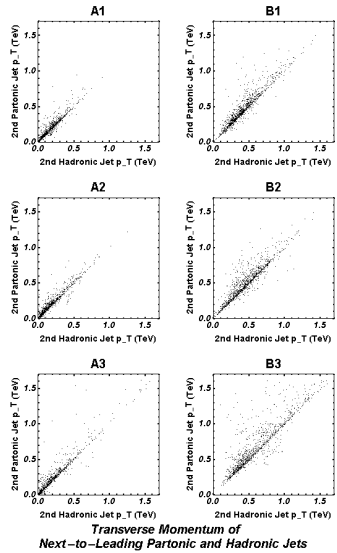


FIG. 39: As in Fig. 35, for the k_T algorithm with R parameter 0.52 (see Table IV.)

- [7] A. Delgado, J. R. Espinosa and M. Quiros, JHEP **0710**, 094 (2007) [arXiv:0707.4309 [hep-ph]].
- [8] M. J. Strassler, arXiv:0801.0629 [hep-ph].
- [9] R. Schabinger and J. D. Wells, Phys. Rev. D **72**, 093007 (2005) [arXiv:hep-ph/0509209].
- [10] M. Bowen, Y. Cui and J. D. Wells, JHEP **0703**, 036 (2007) [arXiv:hep-ph/0701035].
- [11] S. Gopalakrishna, S. Jung and J. D. Wells, arXiv:0801.3456 [hep-ph],
- [12] J. R. Espinosa and M. Quiros, Phys. Rev. D **76**, 076004 (2007) [arXiv:hep-ph/0701145].
- [13] J. March-Russell, S. M. West, D. Cumberbatch and D. Hooper, arXiv:0801.3440 [hep-ph].
- [14] M. J. Strassler and K. M. Zurek, Phys. Lett. B **661**, 263 (2008) [arXiv:hep-ph/0605193].
- [15] M. J. Strassler, arXiv:hep-ph/0607160.
- [16] T. Han, Z. Si, K. M. Zurek and M. J. Strassler, arXiv:0712.2041 [hep-ph].
- [17] S. Chang, P. J. Fox and N. Weiner, JHEP **0608**, 068 (2006) [arXiv:hep-ph/0511250].
- [18] S. Mrenna, P. Skands, M.J. Strassler, in preparation.
- [19] M.J. Strassler, unpublished. I am indebted to S. Mrenna and P. Skands for their advice in constructing this software.
- [20] T. Sjostrand, S. Mrenna and P. Skands, JHEP **0605**, 026 (2006) [arXiv:hep-ph/0603175].
- [21] S. B. Giddings and S. D. Thomas, Phys. Rev. D **65**, 056010 (2002) [arXiv:hep-ph/0106219].
- [22] S. Dimopoulos and G. L. Landsberg, Phys. Rev. Lett. **87**, 161602 (2001) [arXiv:hep-ph/0106295]; G. L. Landsberg, Phys. Rev. Lett. **88**, 181801 (2002) [arXiv:hep-ph/0112061].
- [23] J. Thaler and L. T. Wang, arXiv:0806.0023 [hep-ph]. D. E. Kaplan, K. Rehermann, M. D. Schwartz and B. Tweedie, arXiv:0806.0848 [hep-ph].
- [24] F. Maltoni and T. Stelzer, JHEP **0302**, 027 (2003) [arXiv:hep-ph/0208156].
- [25] S.D. Ellis, M.J. Strassler, C.K. Vermilion and J.R. Walsh, in preparation.
- [26] M.J. Strassler, “Unusual Physics Signatures at the LHC”, presented at the Pheno 2007 Conference, Madison, WI, May 2007.
- [27] S. Mrenna, P. Skands, M.J. Strassler, in preparation.
- [28] P.-A. Delsart, K. Geerlings and J. Huston, unpublished. See www.pa.msu.edu/huston/SpartyJet/SpartyJet.html.
- [29] M. Cacciari and G. P. Salam, Phys. Lett. B **641**, 57 (2006) [arXiv:hep-ph/0512210].
- [30] I am grateful to J.R. Walsh for providing these background samples, which were simulated using MadEvent [24].